Regulatory Toxicology and Pharmacology 70 (2014) 214–221

Contents lists available at ScienceDirect

Regulatory Toxicology and Pharmacology

journal homepage: www.elsevier.com/locate/yrtph

Human plasma concentrations of herbicidal carbamate molinate extrapolated from the pharmacokinetics established in *in vivo* experiments with chimeric mice with humanized liver and physiologically based pharmacokinetic modeling

Masanao Yamashita [a], Hiroshi Suemizu [b], Norie Murayama [a], Sayako Nishiyama [a], Makiko Shimizu [a], Hiroshi Yamazaki [a,*]

[a] *Laboratory of Drug Metabolism and Pharmacokinetics, Showa Pharmaceutical University, Machida, Tokyo 194-8543, Japan*
[b] *Central Institute for Experimental Animals, Kawasaki-ku, Kawasaki 210-0821, Japan*

ARTICLE INFO

Article history:
Received 2 May 2014
Available online 10 July 2014

Keywords:
Physiologically based pharmacokinetic model
Transplanted human liver cells
Lowest-observed-adverse-effect level
Simulation
Allometric scaling

ABSTRACT

To predict concentrations in humans of the herbicidal carbamate molinate, used exclusively in rice cultivation, a forward dosimetry approach was carried out using data from lowest-observed-adverse-effect-level doses orally administered to rats, wild type mice, and chimeric mice with humanized liver and from *in vitro* human and rodent experiments. Human liver microsomes preferentially mediated hydroxylation of molinate, but rat livers additionally produced molinate sulfoxide and an unidentified metabolite. Adjusted animal biomonitoring equivalents for molinate and its primary sulfoxide from animal studies were scaled to human biomonitoring equivalents using known species allometric scaling factors and human metabolic data with a simple physiologically based pharmacokinetic (PBPK) model. The slower disposition of molinate and accumulation of molinate sulfoxide in humans were estimated by modeling after single and multiple doses compared with elimination in rodents. The results from simplified PBPK modeling in combination with chimeric mice with humanized liver suggest that ratios of estimated parameters of molinate sulfoxide exposure in humans to those in rats were three times as many as general safety factor of 10 for species difference in toxicokinetics. Thus, careful regulatory decision is needed when evaluating the human risk resulting from exposure to low doses of molinate and related carbamates based on data obtained from rats.

1. Introduction

Complex, specific, multi-compartment physiologically based pharmacokinetic (PBPK) models for predicting chemical concentrations in various biological fluids in animals and humans can be found in the literature (Edwards and Preston, 2008; McLanahan et al., 2012); however, simple, easy, inexpensive, and/or reliable methods are needed for accurately evaluating chemical toxic risks for humans (McLanahan et al., 2012). We proposed a simple and reliable PBPK model capable of both forward and reverse dosimetry approaches using a three-compartment PBPK model for acrylonitrile (Takano et al., 2010). The developed PBPK model consisted simply of the gut as the chemical absorption compartment, the liver as the metabolizing compartment, and the general circulation as the central compartment.

Furthermore, it was possible to validate the estimates obtained from simplified human PBPK modeling by comparing their results with *in vivo* experimental results from humanized mice transplanted with human liver cells (Hasegawa et al., 2011; Higuchi et al., 2014; Yamazaki et al., 2012). Recently developed TK-NOG (Hasegawa et al., 2011) mice were treated to express a herpes simplex virus type 1 thymidine kinase (HSVtk) within the livers of severely immunodeficient NOG (non-obese diabetes-severe combined immunodeficiency- interleukin-2 receptor gamma chain-deficient) mice and induced by a non-toxic dose of ganciclovir, and human liver cells were transplanted in the absence of ongoing drug treatment. We recently described the use of humanized mice in combination with PBPK modeling for risk assessment of melengestrol acetate (Tsukada et al., 2013). When relevant and reliable estimates of the internal dose of a compound or a key

* Corresponding author. Address: Laboratory of Drug Metabolism and Pharmacokinetics, Showa Pharmaceutical University, 3-3165 Higashi-tamagawa Gakuen, Machida, Tokyo 194-8543, Japan. Fax: +81 42 721 1406.
E-mail address: hyamazak@ac.shoyaku.ac.jp (H. Yamazaki).

http://dx.doi.org/10.1016/j.yrtph.2014.06.028
0273-2300/

metabolite are available, the results of toxicology studies can often be better understood and evaluated in terms of the internal dose.

Molinate (*S*-ethyl hexahydro-1*H*-azepine-1-carbothioate) is a thiocarbamate herbicide widely used on rice fields; it has been reported previously to result in testicular toxicity after metabolic activation via sulfoxidation (Jewell et al., 1998). A preliminary seven-compartment PBPK model for molinate, intended to extrapolate the reproductive risk to humans, has been reported (Campbell, 2009); this model was validated in the rat and then extrapolated to humans. In Campbell's model, the pharmacologically active metabolite sulfoxide is generated in the liver and can circulate in the blood. However, the complicated multiple compartments and equations found in traditional PBPK modeling cause severe difficulties when applying the model for many researchers. Simple and reliable methods are still needed to explore the biological significance of a wide range of chemicals, including thiocarbamate herbicides.

The present study established a simplified PBPK model for molinate in humans; the model was based on physiological parameters derived from the literature, coefficients derived *in silico*, metabolic parameters determined *in vitro* using relevant liver microsomes, and *in vivo* experiment-supported PBPK modeling in rats, wild type mice, and mice with humanized liver. The model was able to estimate some accumulation of molinate sulfoxide after multiple molinate doses in humans for the purpose of evaluating the different molinate exposure levels in humans and rodents in comparison with general safety factor of 10 for species difference in toxicokinetics.

2. Materials and methods

2.1. Chemicals, animals, and enzyme preparations

Male 6-week-old Sprague–Dawley rats (Charles River Laboratory Japan, Tokyo, Japan) and wild type TK-NOG mice (TK-NOG mice with no transplanted human hepatocytes) and chimeric TK-NOG mice with humanized liver (~20–30 g body weight) (Hasegawa et al., 2011) were used in this study. In the chimeric mice, more than 70% of liver cells were estimated to have been replaced with human hepatocytes, as judged by measurements of human albumin concentrations in plasma (Hasegawa et al., 2011; Yamazaki et al., 2012). Hereafter, the terms "mouse" or "mice" refer to wild type TK-NOG mice. Plasma samples were collected 0.5, 1, 2, and 4 h after single oral doses of molinate (250 mg/kg, Wako Pure Chemicals, Tokyo, Japan). For mice, 250 mg/kg of molinate was reported to be the lowest-observed-adverse-effect level (US EPA, MOLINATE – Revised Human Health Risk Assessment, 2001; EC, Health & Consumer Protection Directorate-General: Review report for the active substance molinate, 2003; APVMA, The Reconsideration of Approvals and Registrations Relating to Molinate, Review scope document, 2003; and Food Safety Commission of Japan, Molinate, 2014). The use of animals for this study was approved by the Ethics Committees of Central Institute for Experimental Animals and Showa Pharmaceutical University. Liver microsomes from rats (7-week-old males) and mice were prepared as described previously (Tsukada et al., 2013). Protein concentrations were estimated by using a bicinchoninic acid protein assay kit (Pierce, Rockford, IL, USA). Microsomes from pooled human livers (H150) and recombinant P450 enzymes were obtained from Coning (Woburn, MA, USA). Other reagents used in this study were obtained from sources described previously or were of the highest quality commercially available (Tsukada et al., 2013).

2.2. In vitro and in vivo metabolic studies of molinate

Molinate elimination rates for liver microsomes from rats, wild type mice, humanized mice, and humans were measured using a liquid chromatography (LC) system. Briefly, a typical incubation mixture consisted of 100 mM potassium phosphate buffer (pH 7.4 or 8.4), an NADPH-generating system, molinate (40 μM), and liver microsomes (0.50 mg protein/mL) or recombinant P450 and FMO enzymes (0.80 μM) in a final volume of 0.25 mL. Incubations were carried out at 37 °C for 15 min. Reactions were terminated by adding 0.025 mL of 60% perchloric acid. After vortex mixing, the tubes were centrifuged at 1000*g* for 5 min. Samples (50 μL) were injected with an auto-sampler. Molinate and its metabolites in the incubation mixtures and plasma samples were determined by LC. The LC system consisted of a pump and multi-wavelength UV detector (Shimadzu, Kyoto, Japan) using an analytical C_{18} reversed-phase column (5 μm, 4.6 × 250 mm, Mightysil RP-18 GP, Kanto Chemicals, Tokyo, Japan). The mobile phases were as follows: buffer A contained 100% CH_3CN and buffer B contained 25 mM potassium phosphate buffer (pH 6.6). The following gradient program was used at a flow rate of 1.5 mL/min: 0–25 min, linear gradient from 20% A to 70% A (v/v); 25–35 min, hold at 70% A; 35–45 min, linear gradient from 70% A to 20% A (v/v). The UV detector was set at a wavelength of 230 nm unless otherwise specified. The LC apparatus was operated at room temperature. Metabolites were quantified on the basis of the standard curve peak area at UV 230 nm of molinate.

Statistical analyses of the plasma concentrations of molinate and its metabolites in rats, wild type mice, and humanized mice were done using two-way analysis of variance (ANOVA) with Bonferroni post tests (Prism, GraphPad Software, La Jolla, CA, USA). Area under the curve (AUC) values were derived from plots of molinate and its metabolites versus time and were calculated using the trapezoidal rule with the program WinNonlin (Pharsight, Sunnyvale, CA, USA).

2.3. LC/tandem mass spectrometry assay

A Quattro micro API mass analyzer was used for metabolite analysis (Waters, Tokyo, Japan) using an LC/tandem mass spectrometry (LC–MS/MS) system. The instrument was operated in electrospray positive ionization mode and was directly coupled to the LC 2695 system (Waters) with a C_{18} column (Xbrige, 3.5 μm, 2.1 × 150 mm); MassLynx NT4.1 software was used for data acquisition (Waters). To tune the mass spectrometer, a solution of molinate (10 ppm in a mobile phase) was infused into the ion source, and the cone voltage was optimized to maximize the intensity of the precursor ions for molinate (*m/z* 188.1). The collision energy was then adjusted to optimize the signal for abundant molinate product ions (*m/z* 142.1 and *m/z* 126.1). Typical tuning conditions were as follows: electrospray capillary voltage, 3.2 kV; sample cone voltage, 30 V; and collision energy, 20 eV at a collision gas pressure 1.6×10^{-4} kPa argon.

MS analyses were performed for molinate and its metabolites. LC conditions were as follows: buffer A contained 1.0% CH_3CO_2H in CH_3CN and buffer B contained 1.0% CH_3CO_2H in H_2O (v/v). The following gradient program was used at a flow rate of 0.25 mL/min: 0–20 min, linear gradient from 5% A to 70% A (v/v); 20–25 min, hold at 70% A; 25–26 min, linear gradient from 70% A to 5% A (v/v); until 30 min, hold at 5% A. The temperature of the column was maintained at 40 °C. Samples (10 μL) were injected with an auto-sampler. MS analyses were performed for molinate and its metabolites. Molinate, molinate sulfoxide, and hydroxymolinate were analyzed using the *m/z* 188.1 → 126.1 transition of molinate, the *m/z* 204.2 → 126.1 transition of molinate sulfoxide, and the *m/z* 204.2 → 142.1 transition of hydroxymolinate.

2.4. Estimation of plasma concentrations of molinate and molinate sulfoxide using a PBPK model with suitable parameters

A simplified PBPK model was set up as described previously (Gargas et al., 1995; Kato et al., 2008; Takano et al., 2010;

Table 1
Chemical properties of molinate and molinate sulfoxide (M1).

Parameter	Symbol	Molinate	Molinate sulfoxide
Molecular weight	MW	187	203
Octanol–water partition coefficient	logP	2.85	1.50
Plasma unbound fraction	$f_{u,p}$	0.137	0.390
Fraction unbound in microsomes	$f_{u,mic}$	0.635	0.898
Blood to plasma concentration ratio	R_b	0.860	0.923
Liver to plasma concentration ratio	$K_{p,h}$	2.56	0.928

Molinate sulfoxide was identified in this study (Fig. 2).

Tsukada et al., 2013; Yamazaki et al., 2010). The model essentially consisted of a chemical receptor compartment, a metabolizing compartment, and a central compartment. The physicochemical properties of molinate and molinate sulfoxide are shown in Table 1. Values of the plasma unbound fraction ($f_{u,p}$) and the octanol–water partition coefficient (logP) were obtained by *in silico* estimation using SimCYP and ChemDrawBioUltra software (Emoto et al., 2009); the liver to plasma concentration ratio ($K_{p,h}$) and the blood to plasma concentration ratio (R_b) were estimated from $f_{u,p}$ and logP (Tsukada et al., 2013). Values of the fraction unbound in microsomes ($f_{u,mic}$) (0.635) and $f_{u,p}$ (0.137) of molinate were experimentally confirmed by LC measurements of ultrafiltrates from 1.0 and 40 mg/mL of bovine serum albumin solution in 50 mM Tris HCl buffer (pH 7.4). Parameters that represent physiological properties such as hepatic volumes and blood flow rates in rats, mice, and humans were taken from the literature (Gargas et al., 1995; Kato et al., 2008).

Experimental plasma concentrations of molinate and its metabolites were analyzed using WinNonlin software (Professional version 5.2.1) with a one-compartment model and yielded primary absorption rate constant (k_a) and elimination constant (k_{el}) values as pharmacokinetic parameters. Values of the total clearance (CL_{tot}), hepatic clearance (CL_h), hepatic intrinsic clearance ($CL_{h,int}$), and the volume of the systemic circulation (V_1) were also calculated (Tsukada et al., 2013). Subsequently, using the initial values mentioned above, final parameter values for the rat and mouse PBPK models were calculated by the user model in WinNonlin; these parameters are shown in Tables 1 and 2. Consequently, the following system of differential equations was solved to conduct the modeling for molinate:

$$\frac{dX_g(t)}{dt} = -k_a \cdot X_g(t) \quad \text{where at} \quad t = 0, X_g(0) = dose \tag{1}$$

$$V_h \frac{dC_h}{dt} = Q_h \cdot C_b - \frac{Q_h \cdot C_h \cdot R_b}{K_{p,h}} + k_a \cdot X_g - CL_{h,int} \cdot \frac{C_h}{K_{p,h}} \cdot f_{u,p} \tag{2}$$

$$V_1 \frac{dC_b}{dt} = -Q_h \cdot C_b + \frac{Q_h \cdot C_h \cdot R_b}{K_{p,h}} - CL_r \cdot C_b \tag{3}$$

where X_g is the amount of molinate in the gut, C_h is the hepatic molinate concentration, and C_b is the blood molinate concentration.

For the metabolite:

$$V_1 \frac{dC_b}{dt} = -Q_h \cdot C_b + \frac{Q_h \cdot C_h \cdot R_b}{K_{p,h}} - CL_r \cdot C_b \tag{4}$$

$$V_h \frac{dC_h}{dt} = Qh \cdot C_b - \frac{Q_h \cdot C_h \cdot R_b}{K_{p,h}} - CL_{h,int} \cdot \frac{C_h}{K_{p,h}} \cdot f_{u,p} + CL_{h,int,metabolite} \cdot \frac{C_{h,metabolite}}{K_{p,h,metabolite}} \cdot f_{u,p,metabolite} \tag{5}$$

To define a simplified PBPK model for molinate and its metabolite in humans based on the rat or mouse PBPK model, we used relevant liver microsomes and physiological parameters (CL_r, k_a, and V_1) derived from the literature and applied the systems

Table 2
Physiological, experimental, and calculated parameters for the PBPK models of molinate disposition in rats, wild type mice, humanized mice, and humans.

Parameter	Symbol (unit)	Rat	Rat extrapolated from literature[a]	Wild type mouse	Humanized mouse	Human, extrapolated from rat	Human, extrapolated from wild type mouse	Human, extrapolated from humanized mouse
Body weight	BW (kg)	0.25	0.25	0.025	0.025	70	70	70
Liver weight	Liver weight (g)	10	10	1.5	1.5	1500	1500	1500
Hepatic blood flow rate of systemic circulation to the tissue compartment	Q_h (L/h)	0.853	0.853	0.160	0.160	96.6	96.6	96.6
Volume of liver	V_h (L)	0.00850	0.00850	0.000850	0.000850	1.50	1.50	1.50
Volume of blood	V_b (L)	0.0160	0.0160	0.00160	0.00160	4.90	4.90	4.90
Absorption rate constant	k_a (1/h)	5.04	67.3	1.28	1.39	3.75	0.950	1.04
Fraction absorbed × intestinal availability	F_aF_g	1	1	1	1	1	1	1
Hepatic availability	F_h	0.077	0.077	0.575	0.480	0.121	0.248	0.184
Volume of systemic circulation for molinate	$V_{1\_molinate}$ (L)	5.13	1.82	0.192	0.0800	1440	541	227
Hepatic clearance for molinate	$CL_{h,molinate}$ (L/h)	0.787	0.914	0.0725	0.112	84.9	56.9	76.6
Hepatic intrinsic clearance for molinate	$CL_{h,int\_molinate}$ (L/h)	63.9	64.1	0.833	2.33	4400	871	2330
Metabolic ratio to M1		0.30	0.30	0.70	0.80	0.35	0.35	0.80
Renal clearance for molinate	$CL_{r\_molinate}$ (L/h)	0	0	0	0	0	0	0
Volume of systemic circulation for metabolite M1	V_{1_M1} (L)	4.26	1.82	0.0297	0.0300	1190	84.6	85.3
Hepatic clearance for metabolite M1	$CL_{h,M1}$ (L/h)	0.275	0.914	0.0134	0.0122	21.6	13.2	11.6
Hepatic intrinsic clearance for metabolite M1	CL_{h,int_M1} (L/h)	0.958	64.1	0.0347	0.0313	65.9	36.3	31.3
Renal clearance for metabolite M1	CL_{r_M1} (L/h)	0	0	0	0	0	0	0

Some other parameters are shown in Table 1; M1, molinate sulfoxide, as identified in Fig. 2.
[a] Taken form Campbell, 2009.

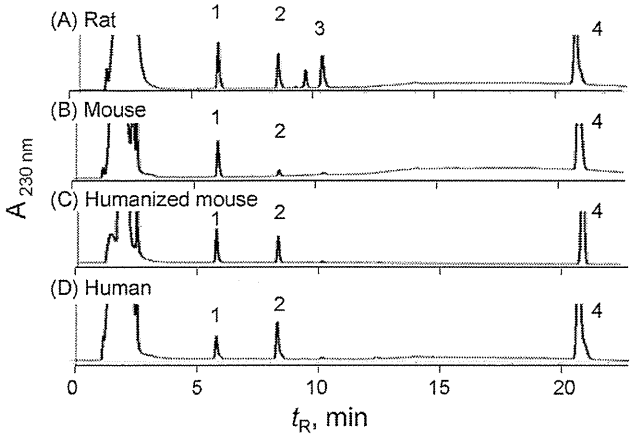

Fig. 1. Representative chromatograms for *in vitro* metabolites of molinate produced by liver microsomes from rats (A), wild type mice (B), humanized livers transplanted into chimeric mice (C), and pooled human livers (D). Molinate (40 μM) was incubated with liver microsomes (0.50 mg/mL) at 37 °C for 15 min. Extracted metabolites were separated with reverse-phase LC. Peak 1, molinate sulfoxide (see Fig. 2, suggested by LC–MS/MS along with information found in the literature); peak 2, hydroxymolinate (see Fig. 2); peak 3, unidentified; peak 4, molinate (see Fig. 2). The metabolites were quantified on the basis of the standard curve peak area at UV 230 nm of molinate (see Table 3).

approach to fit them into the traditional parallelogram for risk assessment (Edwards and Preston, 2008). The values of CL_h, k_a, and V_1 in the human PBPK model were estimated using a scale-up strategy from rats and mice to humans as described previously (Tsukada et al., 2013). The human hepatic (or renal) clearance $CL_{,human}$ was estimated using Eq. (6), where BW_{rodent} = 0.25 (rat) or 0.025 (mouse) kg and BW_{human} = 70 kg:

$$CL_{h,human} = \frac{CL_{h,rodent}}{BW_{rodent}^{(\frac{2}{3})}} \cdot BW_{human}^{(\frac{2}{3})} \quad (6)$$

The human absorption rate constant (k_a) was estimated as (Amidon et al., 1988):

$$K_{a,human} = 0.744 \cdot k_{a,rodent} \quad (7)$$

The human systemic circulation volume ($V_{1,human}$) was estimated from Eqs. (8) and (9), where $V_{h,human}$, $V_{b,rodent}$, and $V_{b,human}$ were 1.50 L, 0.0160 (rat) and 0.00160 (mouse) L, and 4.90 L, respectively:

$$V_{d,human} = V_{b,human} + (V_{d,rodent} - V_{b,rodent}) \cdot \frac{R_{b,rodent}}{f_{u,p,rodent}} \cdot \frac{f_{u,p,human}}{R_{b,human}} \quad (8)$$

$$V_{1,human} = V_{d,human} - V_{h,human} \cdot \frac{K_{p,h}}{R_b} \cdot F_h \quad (9)$$

where physicochemical parameters such as $K_{p,h}$, R_b, and $f_{u,p}$ were assumed to be the same for rats and humans (Tsukada et al., 2013). V_d is the distribution volume.

Table 4
Rates of metabolite formation and molinate elimination determined using recombinant human P450 and FMO enzymes.

Enzyme source	Metabolite formation (min^{-1})			Molinate elimination (min^{-1})
	M1[a]	M2	M3	
1A2	21.2	3.3	<0.1	26.4
2B6	24.6	9.2	<0.1	55.6
2C9	<0.1	<0.1	<0.1	<0.1
2C19	<0.1	<0.1	<0.1	<0.1
2D6	<0.1	<0.1	<0.1	<0.1
2E1	<0.1	<0.1	<0.1	<0.1
3A4	28.8	<0.1	<0.1	31.1
FMO1	<0.1	<0.1	<0.1	<0.1
FMO3	<0.1	<0.1	<0.1	<0.1

[a] M1, molinate sulfoxide; M2, hydroxymolinate, as identified in Fig. 2. M3, an unknown metabolite. Molinate (40 μM) was incubated with liver microsomes (0.50 mg/mL) and recombinant human P450 or FMO (0.80 nmol/mL) at 37 °C for 15 min. Extracted metabolites were separated using reverse-phase LC.

The *in vivo* hepatic intrinsic clearance ($CL_{h,int}$) of molinate in humans was estimated by multiplying the calculated initial parameters for *in vitro* hepatic intrinsic clearance values in humans by the ratio of *in vivo* to *in vitro* hepatic intrinsic clearance in rats or mice, as mentioned above for modeling in rats and mice. Then, the final parameters for the human PBPK model were calculated using these initial values by the user model in WinNonlin; these parameters are shown in Table 2. As was done for the rat and mouse models, systems of differential equations were solved to determine the concentrations in each compartment in humans.

3. Results

3.1. Metabolism of molinate

The *in vitro* metabolism of molinate was investigated using liver microsomes from pooled human livers, rats, wild type mice, and chimeric mice with humanized liver. Typical chromatograms are shown in Fig. 1 after the incubation of molinate (40 μM) with liver microsomes; three metabolite peaks (designated as peaks 1–3 in Fig. 1) and peak 4 (assigned to molinate) were observed. The three metabolites were present in different proportions in all reaction mixtures. The rates of metabolite formation and molinate elimination were determined (Table 3). Liver microsomes from rats formed M1, M2, and M3 at roughly similar rates, but human liver microsomes preferentially produced M2. Liver microsomes prepared from transplanted human hepatocytes in chimeric mice mainly catalyzed M1 and M2 formation. Based on the molinate elimination rates in these liver microsomes, hepatic intrinsic clearance ($CL_{h,int,in\ vitro}$) rates were calculated (Table 3) from the elimination rates, substrate concentration, and unbound fractions ($f_{u,mic}$) of

Table 3
Rates of metabolite formation, molinate elimination, and hepatic intrinsic clearance ($CL_{h,int,in\ vitro}$) determined using liver microsomes from pooled human livers, rats, wild type mice, and chimeric mice with humanized liver.

Enzyme source	Metabolite formation (nmol/min/mg protein)			Molinate elimination (nmol/min/mg protein)	$CL_{h,int,in\ vitro}$ (L/h)
	M1[a]	M2	M3		
Human	0.220	0.431	<0.01	0.651	92.2
Rat	0.573	0.422	0.425	1.42	1.34
Wild type mouse	0.419	0.158	<0.01	0.622	0.0882
Chimeric mouse	0.444	0.410	<0.01	0.854	0.121[b]/121[c]

Molinate (40 μM) was incubated with liver microsomes (0.50 mg/mL) at 37 °C for 15 min. Extracted metabolites were separated with reverse-phase LC. Estimated clearance values ($CL_{h,int,in\ vitro}$) were extrapolated using the fraction unbound in liver microsomes and the following values: 40 mg liver microsomal protein per 1 g liver and 10 g liver weight per 0.25 kg of rat BW, 1.5 g liver weight per 0.025 kg of mouse BW, or 1.5 kg liver weight per 70 kg of human BW.
[a]M1, molinate sulfoxide; M2, hydroxymolinate, as identified in Fig. 2. M3, an unknown metabolite. Two CLh,int,in vitro values are shown according to mouse[b] or human[c] liver sizes.

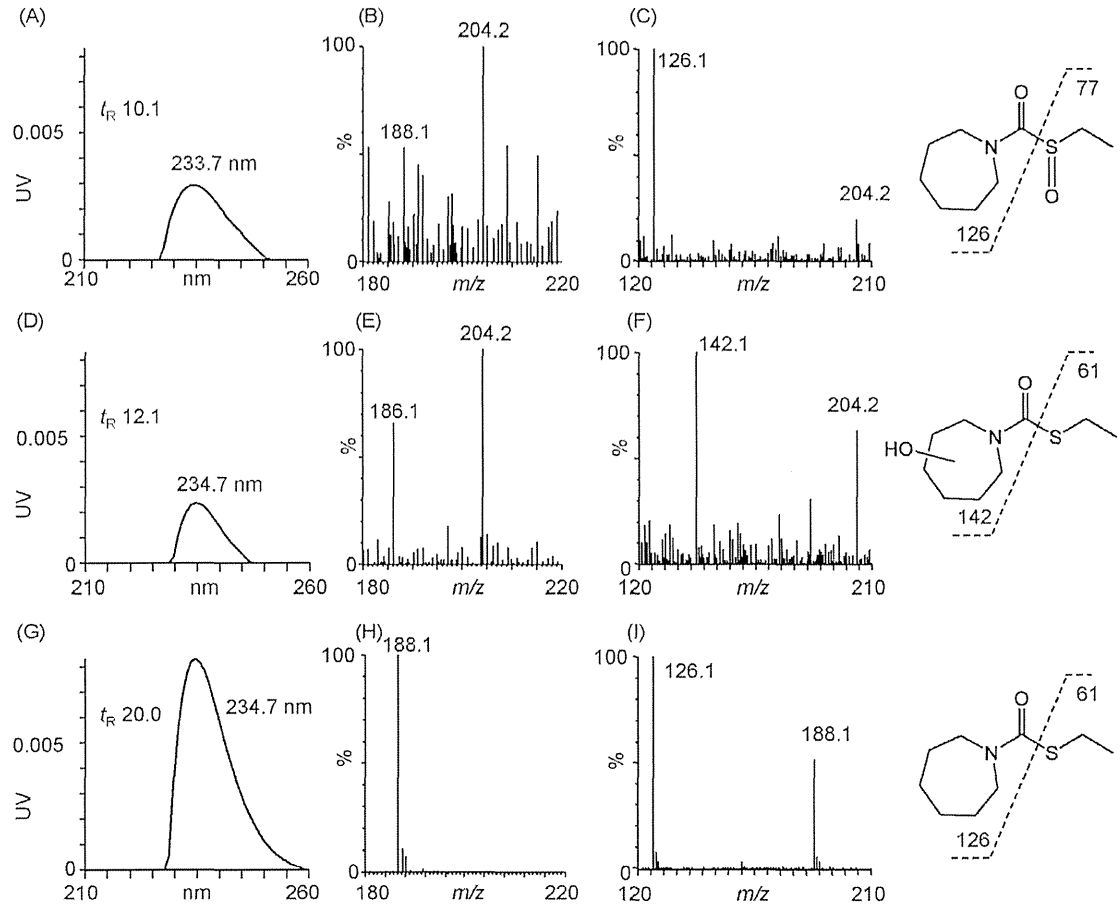

Fig. 2. UV spectra (A,D,G), LC–MS spectra (B,E,H), and LC–MS/MS chromatograms (C,F,I) of molinate sulfoxide (A–C), hydroxymolinate (D–F), and substrate molinate (G–I) in human liver microsomes. Results are shown for incubation mixtures with human liver microsomes and molinate (see Fig. 1).

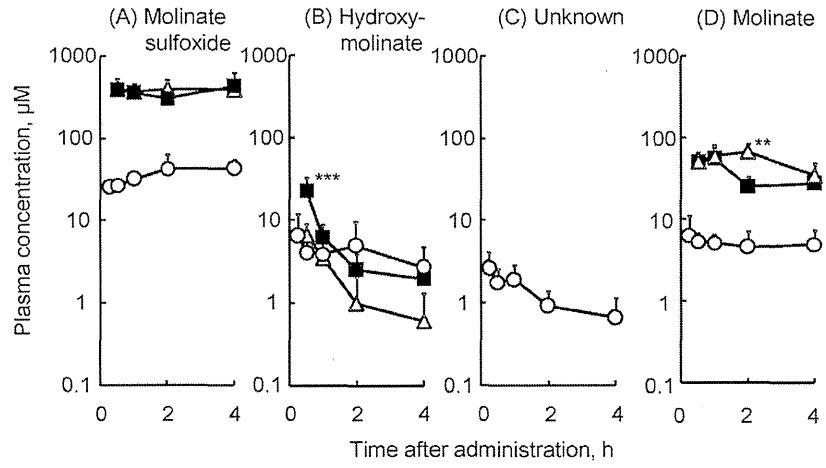

Fig. 3. Measured plasma concentrations of molinate (D) and its three metabolites (A–C) in rats (open circles) and mice with humanized liver (closed squares) and without humanized liver (open triangles) after single oral molinate doses of 250 mg/kg. Data points with bars represent observed means ± SDs of plasma molinate and metabolite concentration in rats, mice with and without humanized liver for five animals after single oral administration of molinate (250 mg/kg). (**$p < 0.01$, ***$p < 0.001$, two-way ANOVA).

0.635 determined by SimCYP software for use in the PBPK models. Estimated clearance values ($CL_{h,int,in\ vitro}$) were extrapolated using the following values: 40 mg liver microsomal protein per 1 g liver and 10 g liver weight per 0.25 kg of rat BW, 1.5 g liver weight per 0.025 kg of mouse BW, or 1.5 kg liver weight per 70 kg of human BW. For example, human $CL_{h,int,in\ vitro}$ value of 92.2 L/h (Table 3) was obtained by the following calculation: 0.651 (nmol/min/mg protein)/(40 × 0.635 (μmol/L) × 60 min/h × 40 (mg protein/g liver) × 1500 (g liver). Among the recombinantly expressed human P450 isoforms tested, P450 1A2, 2B6, and 3A4 preferentially catalyzed the transformation of molinate to M1 (Table 4).

The metabolites seen as peaks 1 and 2 in the reaction mixtures with human livers (Fig. 3) were analyzed using UV and LC–MS spectra and the results were compared with those of molinate

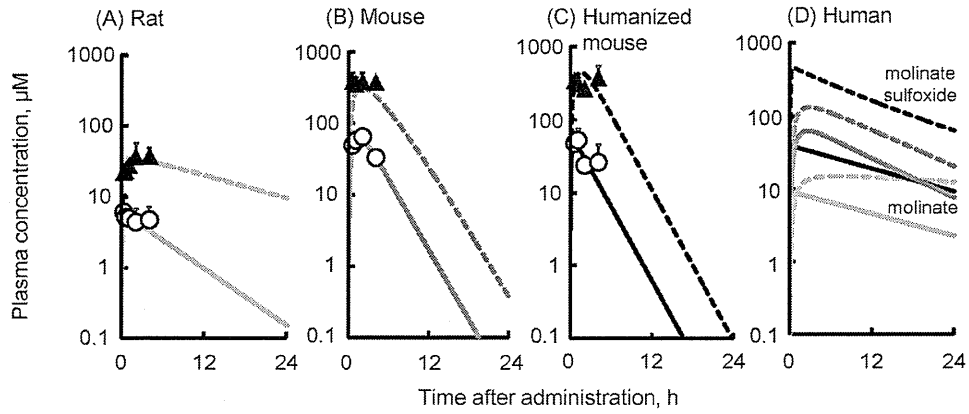

Fig. 4. Measured (symbols) and PBPK-modeled (lines) plasma concentrations of molinate (circles, solid lines) and molinate sulfoxide (triangles, dashed lines) in rats (A), wild type mice (B), humanized mice (C), after oral administration of 250 mg/kg molinate, a lowest-observed-adverse-effect dose. PBPK-modeled plasma concentrations in humans for the same dose of molinate (D). Data points with bars represent experimental means ± SDs obtained from four or five animals. The lines show chemical concentrations estimated using the PBPK model. In panel D, light gray lines, for humans extrapolated from rats; dark gray lines, humans extrapolated from wild type mice; black lines, humans extrapolated from chimeric mice with humanized liver.

(Fig. 2). As shown in Fig. 2A, metabolite M1 resulted in the UV spectra change from a maximum peak of 234.7 nm to 233.7 nm, suggesting a changed moiety in the main chemical structure. The parent ions of M1 and M2 had a molecular weight of 204 (Fig. 2B and E), indicating that one oxygen atom had been introduced to the molinate molecule (a molecular weight of 188, Fig. 2H). In the MS/MS analysis, molinate and M1 both produced peaks at *m/z* 126 (Fig. 2C and I) by losing the SCH_2CH_3-group; hydroxylation of the seven-membered ring structure was suggested in M2 with extraction of a 142 *m/z* ion, as shown in Fig. 2F. Based on several aspects of the present evidence and reported findings, peaks 1 and 2 in the *in vitro* human liver microsomal system were assigned as molinate sulfoxide and hydroxymolinate, respectively.

3.2. Human PBPK model supported by hepatic clearance experiments

To obtain detailed kinetic parameters, male rats, wild type mice, and chimeric mice were orally administered 250 mg/kg of molinate (the lowest-observed-adverse-effect level). Fig. 3 shows the mean levels of molinate and metabolites in plasma from rats, wild type mice, and chimeric mice. Absorbed molinate (Fig. 3D), molinate sulfoxide (Fig. 3A), hydroxymolinate (Fig. 3B), and an unidentified rat-specific metabolite (Fig. 3C) were detected *in vivo* under the present conditions. Chimeric mice with humanized liver had a high hydroxymolinate concentration and a slow elimination curve for molinate. Based on these *in vivo* experiments, the kinetic parameters for molinate and the primary sulfoxide metabolite in rats, wild type mice, and chimeric mice were calculated and are shown in Table 2. Consequently, the final parameters such as the hepatic intrinsic clearance ($CL_{h,int}$), the volume of the systemic circulation (V_1), and the absorption rate constant (k_a) for the rat, wild type mouse, and chimeric mouse PBPK models (consisting essentially of a chemical receptor compartment, a metabolizing compartment, and a central compartment) were obtained as described in the Materials and methods section.

By solving the equations that make up the PBPK models, the plasma concentration curves of molinate and molinate sulfoxide were generated; the resulting estimated *in silico* concentration curves of molinate and molinate sulfoxide are shown with the *in vivo* experimental data in Fig. 4A–C. According to the algometric scaling method for physiological parameters and the derived values shown in Table 2, the human PBPK models for molinate and its main metabolite were set up based on the PBPK models for rats, wild type mice, and mice with humanized liver. The estimated data were produced by the human PBPK model under the linear assumption, as shown in Fig. 4D, because humans were not administered molinate.

Fig. 5 indicates the calculated plasma concentrations after repeated oral administration of molinate (0.21 mg/kg per day, the no-observed-adverse-effect-level dose) using the PBPK models for rats, wild type mice, humanized mice, and humans. The human PBPK model was adopted from the humanized mice model in Fig. 5. The maximum concentrations of molinate were estimated to be

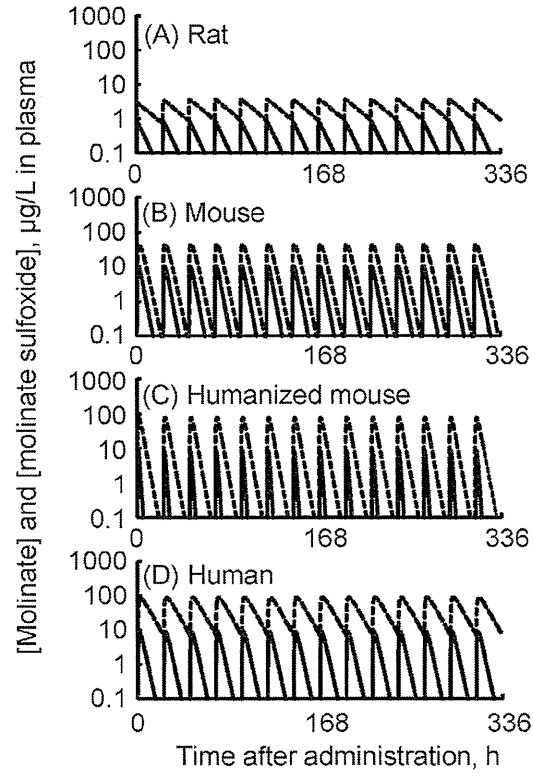

Fig. 5. Concentrations of molinate (solid lines) and molinate sulfoxide (dashed lines) estimated using PBPK models in rats (A), wild type mice (B), humanized mice (C), and humans (D) after multiple oral administrations of molinate (0.21 mg/kg per day, a no-observed-adverse-effect-level dose).

Table 5
Comparison of the modeled peak plasma concentration (C_{max}) and AUC values in rats and humans after single or 14-day oral administrations of a no-observed-adverse-effect-level dose of molinate (0.21 mg/kg per day).

Species	Molinate				Molinate sulfoxide			
	Single		14-days		Single		14-days	
	C_{max}	AUC	$C_{ss,max}$	AUC	C_{max}	AUC	$C_{ss,max}$	AUC
Rat	0.824	5.90	0.846	84.6	2.39	32.9	3.12	584
Human	9.05	46.5	9.06	652	84.9	922	89.8	13400
Human/rat ratio	11.0	7.9	10.7	7.7	35.5	28.0	28.7	23.0

C_{max}, μg/L; AUC, μg h/L.

approximately 1–10 ng/mL in rats, wild type mice, humanized mice, and humans. When daily administration for 14 days of the no-observed-adverse-effect-level dose of molinate was modeled, metabolite accumulations (~10–100 ng/mL) were evident in humans using the present PBPK models (Fig. 5D). Typical kinetic parameters for accumulated molinate and its sulfoxide in humans are shown in Table 5. Ratios of estimated C_{max} and AUC values of molinate after single and multiple doses in humans over rats were approximately 10 (Table 5). In contrast, these ratios of molinate sulfoxide were estimated to be 23- to 36-fold in humans compared with those in rats, implying three-time higher than the general safety factor of 10 for species difference in toxicokinetics.

4. Discussion

The herbicidal carbamate molinate was cleared from plasma of rats, wild type mice, and humanized mice with multiple oxidation pathways *in vitro* and *in vivo* (Figs. 1 and 3). Rat livers rapidly metabolized molinate, as evidenced by the low plasma molinate concentrations in rats compared with those in wild type mice or humanized mice (Fig. 3). A high rate of formation of minor metabolite hydroxymolinate (Fig. 2) in human livers was suggested by *in vitro* and *in vivo* experiments with human liver microsomes, recombinant human P450 2B6, and/or chimeric mice with humanized liver (Tables 3 and 4 and Fig. 3) at the substrate concentration relevant to maximum concentrations under the present *in vivo* experiments; however, the clearance from human plasma was estimated to be lower than that in rats (Fig. 4). Consequently, accumulation of the primary pharmacologically active metabolite molinate sulfoxide was seen in chimeric mice with humanized liver (Fig. 3) and was predicted by human PBPK modeling at a no-observed-adverse-effect-level molinate dose (Fig. 5).

The present study defined a simplified PBPK model for molinate in humans; the model was based on physiological parameters derived from the literature, coefficients derived *in silico*, metabolic parameters determined *in vitro* using relevant liver microsomes, and *in vivo* experiment-supported PBPK modeling in chimeric mice with humanized liver (Tables 1 and 2). In this context, it would be interesting to estimate molinate disposition in humans using full "bottom-up" mechanistic modeling such as a population-based absorption, distribution, metabolism, and excretion simulator (Jamei et al., 2009).

In terms of risk evaluation of molinate, to determine the no-observed-adverse-effect level, *in vivo* rat toxicity data (0.21 mg/kg per day) were adopted and divided by 100 to yield 0.0021 mg/kg per day of daily acceptable intake for humans (Food Safety Commission of Japan, Molinate, 2014). The present results indicated that the disposition of molinate was slow in humans (adopted from the humanized mice model) compared with that in rats, although the rat was selected as the species for determining the important no-observed-adverse-effect level. Ratios of internal exposure of molinate sulfoxide as judged by C_{max} and AUC were estimated to be 29-fold (a mean of 23- to 36-fold) in humans compared with those in rats (Table 5). When extrapolating no-observed-adverse-effect levels from rats to humans, it is generally recognized that a general factor of 10 is usually applied for species differences in toxicokinetics (4) and toxicodynamics (2.5) (Renwick, 1993); however, an additional factor of three seems justified when setting safe exposure levels of molinate for humans, as evidenced by the modeled plasma levels for rats and humans shown in Table 5 after single or 14-days treatments.

In conclusion, a simplified PBPK model for molinate and its primary metabolite was developed using a combination of algorithms, *in vivo* experimentation with chimeric mice with humanized livers, and literature resources. According to the present PBPK analysis, molinate and its active metabolite sulfoxide cleared more slowly from plasma in humans than in rats. The present study indicates that careful consideration is required when applying the forward dosimetry approach to molinate for risk evaluations at the no-observed-adverse-effect level.

Conflict of interest

The authors declare that there are no conflicts of interest.

Acknowledgments

The authors thank Drs. Miyuki Kuronuma, Yasuhiko Ando, and Ryohji Takano for their technical assistance. This work was supported in part by JCIA's LRI program.

References

Amidon, G.L., Sinko, P.J., Fleisher, D., 1988. Estimating human oral fraction dose absorbed: a correlation using rat intestinal membrane permeability for passive and carrier-mediated compounds. Pharm. Res. 5, 651–654.
Campbell, A., 2009. Development of PBPK model of molinate and molinate sulfoxide in rats and humans. Regul. Toxicol. Pharmacol. 53, 195–204.
Edwards, S.W., Preston, R.J., 2008. Systems biology and mode of action based risk assessment. Toxicol. Sci. 106, 312–318.
Emoto, C., Murayama, N., Rostami-Hodjegan, A., Yamazaki, H., 2009. Utilization of estimated physicochemical properties as an integrated part of predicting hepatic clearance in the early drug-discovery stage: impact of plasma and microsomal binding. Xenobiotica 39, 227–235.
Gargas, M.L., Andersen, M.E., Teo, S.K.O., Batra, R., Fennell, T.R., Kedderis, G.L., 1995. A physiologically based dosimetry description of acrylonitrile and cyanoethylene oxide in the rat. Toxicol. Appl. Pharmacol. 134, 185–194.
Hasegawa, M., Kawai, K., Mitsui, T., Taniguchi, K., Monnai, M., Wakui, M., Ito, M., Suematsu, M., Peltz, G., Nakamura, M., Suemizu, H., 2011. The reconstituted 'humanized liver' in TK-NOG mice is mature and functional. Biochem. Biophys. Res. Commun. 405, 405–410.
Higuchi, Y., Kawai, K., Yamazaki, H., Nakamura, M., Bree, F., Guillouzo, C., Suemizu, H., 2014. The human hepatic cell line HepaRG as a possible cell source for the generation of humanized liver TK-NOG mice. Xenobiotica 44, 146–153.
Jamei, M., Dickinson, G.L., Rostami-Hodjegan, A., 2009. A framework for assessing inter-individual variability in pharmacokinetics using virtual human populations and integrating general knowledge of physical chemistry, biology, anatomy, physiology and genetics: a tale of 'bottom-up' versus 'top-down' recognition of covariates. Drug Metab. Pharmacokinet. 24, 53–75.
Jewell, W.T., Hess, R.A., Miller, M.G., 1998. Testicular toxicity of molinate in the rat: metabolic activation via sulfoxidation. Toxicol. Appl. Pharmacol. 149, 159–166.

Kato, M., Shitara, Y., Sato, H., Yoshisue, K., Hirano, M., Ikeda, T., Sugiyama, Y., 2008. The quantitative prediction of CYP-mediated drug interaction by physiologically based pharmacokinetic modeling. Pharm. Res. 25, 1891–1901.

McLanahan, E.D., El-Masri, H.A., Sweeney, L.M., Kopylev, L.Y., Clewell, H.J., Wambaugh, J.F., Schlosser, P.M., 2012. Physiologically based pharmacokinetic model use in risk assessment – why being published is not enough. Toxicol. Sci. 126, 5–15.

Renwick, A.G., 1993. Data derived safety factors for the evaluation of food additives and environmental contaminants. Food Addit. Contam. 10, 275–305.

Takano, R., Murayama, N., Horiuchi, K., Kitajima, M., Kumamoto, M., Shono, F., Yamazaki, H., 2010. Blood concentrations of acrylonitrile in humans after oral administration extrapolated from *in vivo* rat pharmacokinetics, *in vitro* human metabolism, and physiologically based pharmacokinetic modeling. Regul. Toxicol. Pharmacol. 58, 252–258.

Tsukada, A., Suemizu, H., Murayama, N., Takano, R., Shimizu, M., Nakamura, M., Yamazaki, H., 2013. Plasma concentrations of melengestrol acetate in humans extrapolated from the pharmacokinetics established in in vivo experiments with rats and chimeric mice with humanized liver and physiologically based pharmacokinetic modeling. Regul. Toxicol. Pharmacol. 65, 316–324.

Yamazaki, H., Horiuchi, K., Takano, R., Nagano, T., Shimizu, M., Kitajima, M., Murayama, N., Shono, F., 2010. Human blood concentrations of cotinine, a biomonitoring marker for tobacco smoke, extrapolated from nicotine metabolism in rats and humans and physiologically based pharmacokinetic modeling. Int. J. Environ. Res. Public Health 7, 3406–3421.

Yamazaki, H., Suemizu, H., Shimizu, M., Igaya, S., Shibata, N., Nakamura, N., Chowdhury, G., Guengerich, F.P., 2012. *In vivo* formation of dihydroxylated and glutathione conjugate metabolites derived from thalidomide and 5-hydroxythalidomide in humanized TK-NOG mice. Chem. Res. Toxicol. 25, 274–276.

Regulatory Toxicology and Pharmacology 70 (2014) 468–473

Contents lists available at ScienceDirect

Regulatory Toxicology and Pharmacology

journal homepage: www.elsevier.com/locate/yrtph

Pharmacokinetics and effects on serum cholinesterase activities of organophosphorus pesticides acephate and chlorpyrifos in chimeric mice transplanted with human hepatocytes

Hiroshi Suemizu [a], Shigeto Sota [b], Miyuki Kuronuma [a], Makiko Shimizu [b], Hiroshi Yamazaki [b,*]

[a] Central Institute for Experimental Animals, Kawasaki-ku, Kawasaki 210-0821, Japan
[b] Laboratory of Drug Metabolism and Pharmacokinetics, Showa Pharmaceutical University, Machida, Tokyo 194-8543, Japan

ARTICLE INFO

Article history:
Received 2 May 2014
Available online 23 August 2014

Keywords:
Transplanted human liver cells
Serum cholinesterase activities
Lowest-observed-adverse-effect level
Physiologically based pharmacokinetic model
Allometric scaling

ABSTRACT

Organophosphorus pesticides acephate and chlorpyrifos in foods have potential to impact human health. The aim of the current study was to investigate the pharmacokinetics of acephate and chlorpyrifos orally administered at lowest-observed-adverse-effect-level doses in chimeric mice transplanted with human hepatocytes. Absorbed acephate and its metabolite methamidophos were detected in serum from wild type mice and chimeric mice orally administered 150 mg/kg. Approximately 70% inhibition of cholinesterase was evident in plasma of chimeric mice with humanized liver (which have higher serum cholinesterase activities than wild type mice) 1 day after oral administrations of acephate. Adjusted animal biomonitoring equivalents from chimeric mice studies were scaled to human biomonitoring equivalents using known species allometric scaling factors and *in vitro* metabolic clearance data with a simple physiologically based pharmacokinetic (PBPK) model. Estimated plasma concentrations of acephate and chlorpyrifos in humans were consistent with reported concentrations. Acephate cleared similarly in humans and chimeric mice but accidental/incidental overdose levels of chlorpyrifos cleared (dependent on liver metabolism) more slowly from plasma in humans than it did in mice. The data presented here illustrate how chimeric mice transplanted with human hepatocytes in combination with a simple PBPK model can assist evaluations of toxicological potential of organophosphorus pesticides.

1. Introduction

Biomonitoring techniques for determining internal doses of chemicals have become valuable tools for quantitatively evaluating human exposure from environmental and/or accidental/incidental sources. The organophosphorus pesticide acephate (Fig. 1) is one of the most widely used pesticides in agriculture. Acephate is bioactivated to the more potent methamidophos, which acts as an acetylcholinesterase inhibitor (Mahajna et al., 1997). There are few case reports of incidental human ingestion of acephate (Chang et al., 2009; Joint FAO/WHO Meeting, 2003). An acetylcholinesterase biosensor has been developed to detect organophosphorus pesticides acephate and malathion in food samples (Raghu et al., 2014).

Chlorpyrifos (Fig. 1), another organophosphorus pesticide, is reportedly extensively activated to chlorpyrifos-oxon and deactivated to trichloropyridinol in rats (Smith et al., 2011; Tang et al., 2001). A benchmark dose analysis (Marty et al., 2012) and meta-analysis (Reiss et al., 2012) have been published for chlorpyrifos and recommended equivalent benchmark doses of 1.7 mg/kg/day for children and adults after a single acute dose and 0.67 mg/kg/day after repeated doses. Physiologically based pharmacokinetic (PBPK) models and/or pharmacodynamic models have been reported for chlorpyrifos, including models for rats and humans (Timchalk et al., 2002), chemical mixtures (Timchalk and Poet, 2008), gestational exposure (Lowe et al., 2009), specific age groups (3 and 30 years) linked to dietary exposure (Hinderliter et al., 2011), predictions of two age groups (1 and 19 years) (Foxenberg et al., 2011), and human life stage (Smith et al., 2014). Dietary exposure levels of chlorpyrifos have been studied extensively.

The complicated multiple compartments and equations found in traditional PBPK modeling cause severe difficulties for many regulatory and industrial researchers when applying the model. Recently developed TK-NOG mice transplanted with human liver

* Corresponding author. Address: Laboratory of Drug Metabolism and Pharmacokinetics, Showa Pharmaceutical University, 3-3165 Higashi-tamagawa Gakuen, Machida, Tokyo 194-8543, Japan. Fax: +81 42 721 1406.
E-mail address: hyamazak@ac.shoyaku.ac.jp (H. Yamazaki).

http://dx.doi.org/10.1016/j.yrtph.2014.08.010
0273-2300/

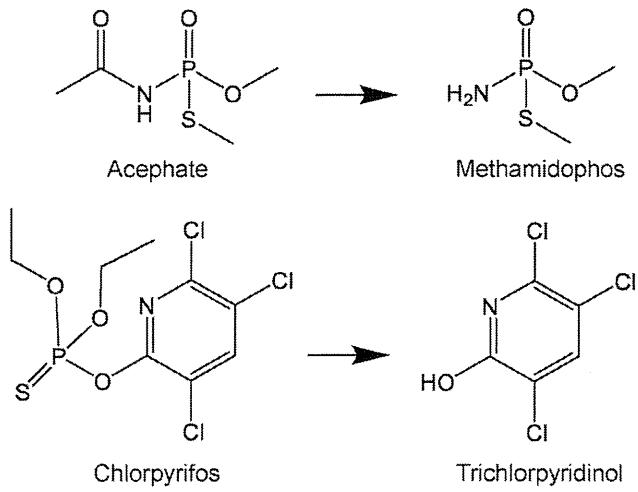

Fig. 1. Chemical structures of acephate and chlorpyrifos and their metabolites.

cells can survive without ongoing drug treatment (Hasegawa et al., 2011; Yamazaki et al., 2013), something that was not possible in previous liver reconstruction animal models. Consequently, with transplanted TK-NOG mice it is now possible to evaluate drug interactions (Yamazaki et al., 2013) and estimates obtained from simplified human PBPK modeling by comparing the predicted values with *in vivo* experimental results from mice with humanized liver. Applying this approach, we reported simplified PBPK models (Tsukada et al., 2013; Yamashita et al., 2014) for estimating the internal doses of melengestrol acetate and molinate and their key metabolites based on data from chimeric mice transplanted with human hepatocytes to better understand and evaluate toxicological studies in humans.

In the present study, the pharmacokinetics of acephate and chlorpyrifos in chimeric mice transplanted with human hepatocytes were investigated. Our observations showed that human hepatocytes were able to elevate serum cholinesterase activities in chimeric mice. A simplified PBPK model was able to estimate human plasma concentrations of acephate and chlorpyrifos after accidental ingestion and was capable of both forward and reverse dosimetry.

2. Materials and methods

2.1. Chemicals, animals, and enzyme preparations

Acephate (*O,S*-dimethyl acetylphosphoramidothioate), methamidophos (*O,S*-dimethyl phosphoramidothioate), chlorpyrifos (*O,O*-diethyl *O*-3,5,6-trichloro-2-pyridyl phosphorothioate), and trichloropyridinol (3,5,6-trichloro-2-pyridinol) were purchased from Wako Pure Chemicals, Tokyo, Japan. Microsomes from pooled human livers (H150) were obtained from Corning (Woburn, MA, USA). Liver microsomes from 7-week-old male Sprague-Dawley rats and mice were prepared as described previously (Tsukada et al., 2013; Yamashita et al., 2014). Recently developed TK-NOG mice (Hasegawa et al., 2011; Higuchi et al., 2014; Yamazaki et al., 2012) are severely immunodeficient NOG (non-obese diabetes-severe combined immunodeficiency interleukin-2 receptor gamma chain-deficient) mice treated to express herpes simplex virus type 1 thymidine kinase (HSVtk) in their livers. Liver cells expressing HSVtk are ablated by a non-toxic dose of ganciclovir, and human liver cells can then be transplanted without the need for ongoing drug treatment. Wild type mice (TK-NOG mice with no transplanted human hepatocytes) and humanized TK-NOG mice (~20–30 g body weight) (Hasegawa et al., 2011) were used in this study. In the chimeric mice, more than 70% of liver cells were estimated to have been replaced with human hepatocytes, as judged by measurements of human albumin concentrations in plasma (Hasegawa et al., 2011; Yamazaki et al., 2012). Hereafter, the terms "mouse" or "mice" refer to wild type TK-NOG mice. The use of animals for this study was approved by the Ethics Committees of the Central Institute for Experimental Animals and Showa Pharmaceutical University. Plasma samples were collected 0.5, 1, 2, 4, 7, and 24 h after single oral doses of acephate (150 mg/kg) or chlorpyrifos (30 mg/kg), these doses being the lowest-observed-adverse-effect levels (Joint FAO/WHO Meeting, 2003). Accumulated urine samples (0–7 h) were also collected. After treatment of the plasma or urine samples (50 μL) from individual mice with methanol (100 μL) for deproteinization, protein concentrations were estimated by using a bicinchoninic acid protein assay kit (Pierce, Rockford, IL, USA). Other reagents used in this study were obtained from sources described previously or were of the highest quality commercially available (Tsukada et al., 2013; Yamashita et al., 2014).

2.2. In vivo and in vitro metabolic studies of acephate and chlorpyrifos

The levels of substrates and their metabolites in plasma samples and in *in vitro* incubation mixtures were determined by liquid chromatography (LC). The levels of acephate and its metabolite in the plasma samples were determined by an LC/tandem mass spectrometry (MS) system as described (Montesano et al., 2007) with modifications. An LCQ Duo mass analyzer (ThermoFisher Scientific, Yokohama, Japan) equipped with Xcalibur software was operated in electrospray positive ionization mode and was directly coupled to an Agilent 1100 system (Agilent Technology, Tokyo, Japan) equipped with an octadecylsilane (C_{18}) column (XBridge, 3.5 μm, 2.1 mm × 150 mm, Waters, Tokyo, Japan). LC conditions were as follows: buffer A contained 5 mM ammonium acetate in methanol and buffer B contained 5 mM ammonium acetate. The following gradient program was used at a flow rate of 0.20 mL/min: 0–6 min, linear gradient from 20% A to 45% A (v/v); 6–7 min, linear gradient from 45% A to 95% A (v/v); 7–12 min, hold at 95% A; 12–13 min, linear gradient from 95% A to 20% A (v/v); 13–19 min, hold at 20% A. The temperature of the column was maintained at 35 °C. Samples (5 μL) were infused with an auto-sampler and MS analyses were performed. To tune the mass spectrometer, solutions of acephate and methamidophos (10 ppm in a mobile phase) were infused into the ion source, and the cone voltage was optimized to maximize the intensity of the precursor ions for the most abundant acephate and methamidophos product ions (*m/z* 184.0 and 142.0, respectively). Acephate and methamidophos were quantified using the *m/z* 184.0 → 142.9 transition of acephate and the *m/z* 142.0 → 112.0 transition of methamidophos. Typical tuning conditions for acephate and methamidophos were as follows: electrospray capillary voltage, 4.5 kV; sample cone voltage, 13 V; collision energy, 33 and 28 eV, respectively; capillary temperature 225 °C; and sheath gas pressure 35 and auxiliary gas pressure 20 (arbitrary units) of helium.

Another LC system, consisting of a pump and multi-wavelength UV detector (Shimadzu, Kyoto, Japan) with an analytical C_{18} reversed-phase column (5 μm, 4.6 × 250 mm, Mightysil RP-18 GP, Kanto Chemicals, Tokyo, Japan), was used for acephate in the following incubation mixtures: solution A contained 5 mM ammonium acetate in methanol and solution B contained 5 mM ammonium acetate in water. The following gradient program was used at a flow rate of 1.0 mL/min: 0–1 min, hold at 5% A; 1–6 min, linear gradient from 5% A to 45% A (v/v); 6–7 min, linear gradient from 45% A to 95% A (v/v); 7–12 min, hold at 95% A; 12–13 min, linear gradient from 95% A to 5% A (v/v); 13–19 min, hold at 5% A.

LC conditions for chlorpyrifos in the plasma samples and *in vitro* incubation mixtures were as follows. Solution A contained CH_3CN

and solution B contained 0.1% CH_3CO_2H in 30% CH_3CN (v/v); the following gradient program was used at a flow rate of 0.80 mL/min: 0–3 min, linear gradient from 0% A to 35% A (v/v); 3–8 min, linear gradient from 35% A to 85% A (v/v); 8–14 min, hold at 85% A; 14–15 min, linear gradient from 85% A to 0% A (v/v); 15–20 min, hold at 0% A. The UV detector was set at a wavelength of 220 nm and 290 nm for acephate and chlorpyrifos, respectively, unless otherwise specified. The LC apparatus was operated at 40 °C. The substrate and metabolite were quantified on the basis of the standard curve peak area.

Elimination rates of acephate and chlorpyrifos mediated by liver microsomes from rats, wild type mice, humanized mice, and humans were measured using an LC system. Briefly, a typical incubation mixture consisted of 100 mM potassium phosphate buffer (pH 7.4), 2 mM $CaCl_2$, an NADPH-generating system, acephate (500 μM) or chlorpyrifos (10 μM), and liver microsomes (0.125–0.50 mg protein/mL) in a final volume of 0.50 mL. Incubations were carried out at 37 °C for 60 and 10 min, respectively, to evaluate the elimination of acephate and chlorpyrifos. Reactions were terminated by adding 0.10–0.50 mL of methanol. After vortex mixing, the tubes were centrifuged at 1000*g* for 5 min. Samples (20–50 μL) were injected with an auto-sampler.

Statistical analyses of the plasma concentrations in mice and humanized mice were done using two-way analysis of variance (ANOVA) with Bonferroni post tests (Prism, GraphPad Software, La Jolla, CA, USA).

2.3. Estimation of plasma concentrations using a PBPK model with suitable parameters

The simplified PBPK model consisted of a chemical receptor compartment, a metabolizing compartment, and a central compartment and was set up as described previously (Takano et al., 2010; Tsukada et al., 2013; Yamashita et al., 2014; Yamazaki et al., 2010). The physicochemical properties of substrates and metabolites are shown in Table 1. Values of the plasma unbound fraction ($f_{u,p}$) and the octanol–water partition coefficient (log*P*) were obtained by *in silico* estimation using SimCYP and ChemDrawBioUltra software (Emoto et al., 2009); the liver to plasma concentration ratio ($K_{p,h}$) and the blood to plasma concentration ratio (R_b) were estimated from $f_{u,p}$ and log*P* (Tsukada et al., 2013; Yamashita et al., 2014). Parameters that represent physiological properties such as hepatic blood flow rates in wild type mice (0.160 L/h) and humans (96.6 L/h) were taken from the literature (Gargas et al., 1995; Kato et al., 2008), respectively. Values of the absorption rate constant (k_a), hepatic clearance (CL_h), hepatic intrinsic clearance ($CL_{h,int}$), and the volume of the systemic circulation (V_1) were also calculated (Tsukada et al., 2013; Yamashita et al., 2014). Renal clearance (CL_r) was calculated as the excreted substrate amounts in urine samples divided by area under the curve (AUC) values from plots of concentrations versus time. Subsequently, final parameter values for the mouse and chimeric mouse PBPK models were calculated using the initial values mentioned above by the user model in WinNonlin; these final parameters are shown in Tables 1 and 2. Finally, a system of differential equations was solved to conduct the modeling (Yamashita et al., 2014).

To define a simplified human PBPK model based on the mouse PBPK model, we used relevant liver microsomes and physiological parameters (CL_r, k_a, and V_1) derived from the literature and applied the systems approach to fit them into the traditional parallelogram for risk assessment (Edwards and Preston, 2008). The values of CL_h, k_a, and V_1 in the human PBPK model were estimated using a scale-up strategy from mice to humans as described previously (Tsukada et al., 2013; Yamashita et al., 2014). The human absorption rate constant (k_a) was estimated as reported (Amidon et al., 1988). The human hepatic (or renal) clearance CL_{human} and the systemic circulation volume ($V_{1,human}$) were estimated using volume of liver (V_h) and volume of blood (V_b), namely $V_{h,human}$, $V_{b,rodent}$, and $V_{b,human}$ values of 1.50 L, 0.00160 L, and 4.90 L, respectively (Tsukada et al., 2013); physicochemical parameters such as $K_{p,h}$, R_b, and $f_{u,p}$ (Tsukada et al., 2013) were assumed to be the same for humans and for mice (Yamashita et al., 2014).

The *in vivo* hepatic intrinsic clearance ($CL_{h,int}$) in humans was estimated by multiplying the calculated initial parameters for *in vitro* hepatic intrinsic clearance values in humans by the ratio of *in vivo* to *in vitro* hepatic intrinsic clearance in mice, as mentioned above for modeling. Then, the final parameters for the

Table 1
Chemical properties of acephate, methamidophos, chlorpyrifos, and trichloropyridinol.

Parameter	Symbol	Acephate	Methamidophos	Chlorpyrifos	Trichloropyridinol
Molecular weight	MW	184	144	350	198
Octanol–water partition coefficient	log*P*	−0.892	−0.868	4.51	1.13
Plasma unbound fraction	$f_{u,p}$	0.883	0.881	0.0277	0.334
Blood to plasma concentration ratio	R_b	0.734	0.736	0.733	0.921
Liver to plasma concentration ratio	$K_{p,h}$	0.714	0.714	6.73	0.702

Table 2
Physiological, experimental, and calculated parameters for PBPK models for acephate and chlorpyrifos in mice, humanized mice, and humans.

Parameters	Symbol (unit)	Acephate			Chlorpyrifos		
		Mouse	Humanized mouse	Human extrapolated	Mouse	Humanized mouse	Human extrapolated
Absorption rate constant	k_a (1/h)	18.5	20.2	15.0	0.471	1.17	0.872
Fraction absorbed × intestinal availability	$F_a \cdot F_g$	1.00	1.00	1.00	1.00	1.00	1.00
Volume of systemic circulation for substrate	V_1 (L)	0.0496	0.0307	87.4	0.301	0.277	778
Hepatic clearance for substrate	CL_h (L/h)	0.00428	0.00239	2.37	0.142	0.123	81.6
Hepatic intrinsic clearance for substrate	$CL_{h,int}$ (L/h)	0.00365	0.00202	2.02	34.1	13.8	13800
Renal clearance for substrate	CL_r (L/h)	0.00974	0.0101	2.06	0	0	0
Metabolic ratio to metabolite		0.500	0.500	0.500	0.770	0.460	0.460
Volume of systemic circulation for metabolite	V_{1_M1} (L)	0.00557	0.0121	35.7	0.0679	0.0264	75.1
Hepatic clearance for metabolite	$CL_{h,M1}$ (L/h)	0.0825	0.0514	42.5	0.00700	0.00300	2.83
Hepatic intrinsic clearance for metabolite	CL_{h,int_M1} (L/h)	0.142	0.0633	63.3	0.0189	0.00805	8.05
Renal clearance for metabolite	CL_{r_M1} (L/h)	0.0679	0.127	25.2	0.000396	0.000282	0.0560

human PBPK model were calculated using these initial values by the user model in WinNonlin; these parameters are shown in Table 2. As was done for the mouse and chimeric mouse models, systems of differential equations were solved to determine the concentrations in each compartment in humans (Yamashita et al., 2014).

3. Results and discussion

3.1. Pharmacokinetics of acephate

In our preliminary observations, transplanted human hepatocytes were able to boost serum cholinesterase activities in chimeric mice (163 U/L compared with 20 U/L in control mice). One day after oral administrations of acephate, 71% inhibition of acetylcholinesterase and/or butyrylcholinesterase was clearly seen in plasma of chimeric mice with humanized liver (Table 3). This level of *in vivo* pharmacological effect of the organophosphorus pesticide was not observed in wild type mice because their cholinesterase activity levels were close to the detection limits in this study. Further detailed study is necessary in this context, but from the viewpoint of species differences, chimeric mice with humanized liver could prove to be a good animal model for determining the pharmacokinetics and also pharmacodynamics of organophosphorus pesticides and for estimating their effects in humans.

Male wild type mice and chimeric mice were orally administered 150 mg/kg acephate, the lowest-observed-adverse-effect-level dose. Fig. 2A shows the mean levels of acephate and its metabolite methamidophos in plasma from wild type mice and chimeric mice. Absorbed acephate and formed methamidophos (Fig. 2A) were detected *in vivo* under the present conditions. Renal clearance values in Table 2 were calculated from the levels of acephate and methamidophos excreted in the accumulated urine samples (9.35 and 0.478 mg, respectively, for wild type mice and 8.68 and 0.653 mg for humanized mice) and from the AUC values (960 and 7.55 mg h/L, respectively, in wild type mice, and 985 and 5.13 mg h/L in humanized mice). The final parameters such as the hepatic intrinsic clearance ($CL_{h,int}$), the volume of the systemic circulation (V_1), and the absorption rate constant (k_a) for the wild type mouse and chimeric mouse PBPK models (consisting essentially of a chemical receptor compartment, a metabolizing compartment, and a central compartment) were obtained as described in Section 2.3. Based on these *in vivo* experiments, the kinetic parameters in wild type mice and chimeric mice were calculated and are shown in Table 2.

The *in vitro* metabolism of acephate was investigated using pooled human liver microsomes and liver microsomes from rats, wild type mice, and chimeric mice with humanized liver. The rates of metabolite formation and substrate elimination were determined (Table 4). Rates of acephate elimination were roughly similar for the liver enzyme sources tested. The formation rates of metabolite

Table 3
Levels of serum butyrylcholinesterase from mice with or without humanized livers before and after oral treatment with acephate.

	Butyrylcholinesterase (U/L)	
	Before treatment	A day after treatment
Control mice	20 (20, 20)	10 (10, 10)
Chimeric mice with humanized liver	163 (160, 165)	48 (45, 50)

Serum levels of butyrylcholinesterase from four mice were measured before and 1 day after treatment with acephate as described in Section 2. Mean and individual values (in parentheses) are shown. Butyrylcholinesterase concentrations in the range 5–500 U/L could be detected.

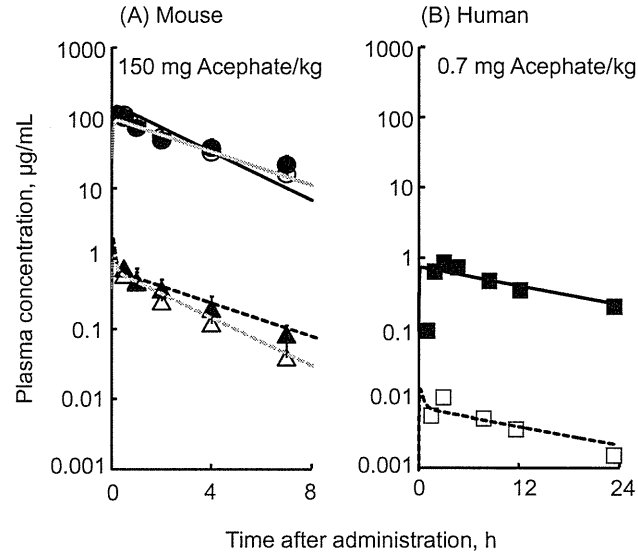

Fig. 2. Measured (A) and reported (B) plasma concentrations of acephate (circles) and its metabolite methamidophos (triangles) in mice with humanized liver (closed symbols) and without humanized liver (open symbols) and in humans after single oral doses of 150 mg/kg (A) and 0.7 mg/kg (B), respectively. Solid and dashed lines show the PBPK model results for acephate and methamidophos, respectively. For the mouse data, gray lines show the results for wild type mice and black lines show the results for humanized mice. For the human data, black lines shows the results of the human PBPK models based on parameters from humanized mice, respectively. Data points with bars represent observed means ± SDs of plasma acephate and methamidophos concentrations in mice with and without humanized liver for five animals after single oral administration of acephate (A). Reported values for acephate (closed) and its metabolite methamidophos (open) in humans for safety analysis are taken from the literature (Joint FAO/WHO Meeting, 2003) (B).

methamidophos were below the detection limit under the present conditions. For mouse PBPK modeling, estimated clearance values were extrapolated using the following values: 40 mg liver microsomal protein per 1 g liver and 1.5 g liver weight per 0.025 kg of mouse body weight (BW) or 1.5 kg liver weight per 70 kg of human BW. Thus, the hepatic intrinsic clearance ($CL_{h,int,in\ vitro}$) rates were calculated based on the substrate elimination rates in these liver microsomes (Table 4).

By solving the equations that make up the PBPK models, plasma concentration curves were created; the resulting estimated *in silico* concentration curves are shown in Fig. 2. There were no large species differences between wild type mice and chimeric mice with humanized livers with respect to *in vivo* acephate pharmacokinetics, including methamidophos formation (Fig. 2). Using the algometric scaling method and the derived values shown in Table 2, human PBPK models for acephate and its metabolite were set up based on the PBPK models for humanized mice. The available reported human data (Joint FAO/WHO Meeting, 2003) obtained after administration of a single low dose of acephate in human subjects could be reasonably estimated by the human PBPK models under the linear assumption, as shown in Fig. 2B.

3.2. Pharmacokinetics of chlorpyrifos

Fig. 3A shows the mean levels of chlorpyrifos and its metabolite trichloropyridinol in plasma from wild type mice and chimeric mice orally administered 30 mg/kg chlorpyrifos. Absorbed chlorpyrifos and formed trichloropyridinol (Fig. 3A) were detected *in vivo* under the present conditions. Chimeric mice with humanized liver had higher chlorpyrifos plasma concentrations than the wild type mice did (Fig. 3A). Renal clearance values in Table 2 were calculated from the levels of trichloropyridinol excreted in the

Table 4
Rates of substrate elimination and metabolite formation determined using liver microsomes from rats, mice, humanized mice, and humans and *in vitro* hepatic intrinsic clearances.

Enzyme source	Acephate elimination, nmol/min/mg protein	Chlorpyrifos and trichloropyridinol, nmol/min/mg protein		$CL_{h,int,in\ vitro}$, L/h	
		Chlorpyrifos elimination	Trichloropyridinol formation	Acephate	Chlorpyrifos
Rat	0.410	2.88	2.80 (0.97)	NA	NA
Wild type mouse	0.630	0.903	0.691 (0.77)	0.00420	0.461
Humanized mouse	0.750	0.520	0.251 (0.48)	0.00520[a]/5.20[b]	0.270[a]/270[b]
Human	0.720	0.333	0.153 (0.46)	4.72	171

Acephate (500 μM) and chlorpyrifos (10 μM) were incubated at 37 °C with liver microsomes (0.125–0.50 mg/mL) for 60 and 10 min, respectively.
Numbers in parentheses are calculated metabolic ratios. Rates of methamidophos formation from acephate were <0.001 nmol/min/mg protein. Hepatic intrinsic clearances ($CL_{h,int,in\ vitro}$) were estimated from elimination rates using the fraction unbound in liver microsomes and the following values: 40 mg liver microsomal protein per 1 g liver and 1.5 g liver weight per 0.025 kg of mouse BW or 1.5 kg liver weight per 70 kg of human BW. Two $CL_{h,int,in\ vitro}$ values are shown according to mouse[a] or human[b] liver sizes.
NA, not available in this study.

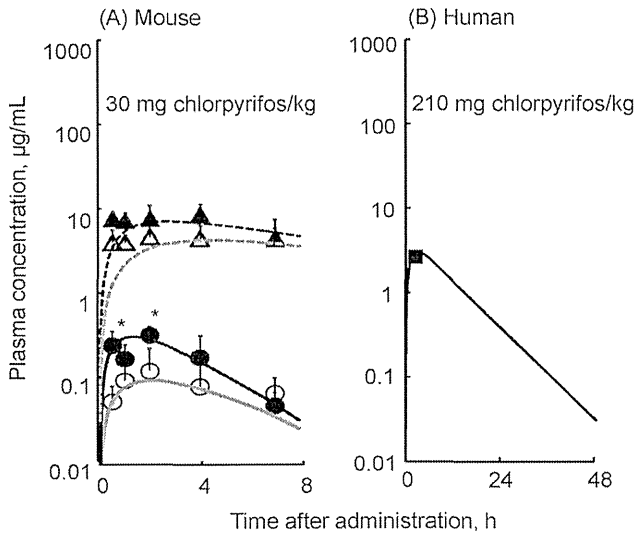

Fig. 3. Measured (A) and reported (B) plasma concentrations of chlorpyrifos (circles) and its metabolite trichloropyridinol (triangles) in mice with humanized liver (closed symbols) and without humanized liver (open symbols) and in humans after single oral doses of 30 mg/kg (A) and 210 mg/kg (B), respectively. Solid and dashed lines show the PBPK model results for chlorpyrifos and trichloropyridinol, respectively. For the mouse data, gray lines show the results for wild type mice and black lines show the results for humanized mice. For the human data, black line shows the results of the human PBPK models based on parameters from humanized mice. Data points with bars represent observed means ± SDs of plasma chlorpyrifos and trichloropyridinol concentrations in mice with and without humanized liver for five animals after single oral administration of chlorpyrifos (*$p < 0.05$, two-way ANOVA). Reported values for chlorpyrifos (closed) in humans are taken from the literature (Drevenkar et al., 1993).

urine samples (0.0351 mg for wild type mice and 0.0340 mg for humanized mice) and from the AUC values (88.5 mg h/L in wild type mice and 121 mg h/L in humanized mice). *In vitro* chlorpyrifos elimination rates mediated by rat and mouse livers were higher than those of human livers (Table 4). The formation of metabolite trichloropyridinol in rat and mouse livers represented 97% and 77% of the substrate elimination, respectively, whereas human and humanized liver microsomes mediated ~50% of the substrate elimination to trichloropyridinol formation under these conditions (Table 4). The final kinetic parameters in wild type mice and chimeric mice were calculated and are shown in Table 2.

A much refined PBPK model for chlorpyrifos has already been published and validated with population data based on farm family studies (Timchalk et al., 2002; Hinderliter et al., 2011; Smith et al., 2014). Occupational/environmental human exposure to chlorpyrifos has been reported (Joint FAO/WHO Meeting, 2003). Under environmental exposure to humans, plasma accumulation at such low exposure levels may not be detectable because of the extremely quick conversion of chlorpyrifos to chlorpyrifos oxon and then to trichloropyridinol, the most stable product. However, the pharmacokinetics of chlorpyrifos in chimeric mice transplanted with human hepatocytes orally administered with a lowest-observed-adverse-effect-level dose suggested slower clearance of chlorpyrifos from plasma in humans than that in mice (Fig. 3).

4. Conclusion

In this study, we investigated the pharmacokinetics of two organophosphorus pesticides, acephate and chlorpyrifos, which were cleared from humanized mice mainly by renal excretion and liver metabolism, respectively. For organophosphorus pesticides dependent on renal clearance, a general factor of 10 could be applied to allow for species differences in toxicokinetics (contributing a factor of 4) and toxicodynamics (contributing a factor of 2.5) (Renwick, 1993). On the other hand, for organophosphorus pesticides dependent on liver clearance, such as chlorpyrifos, an additional toxicokinetic factor will be required in the derivation of safety factors as a result of their slow metabolic clearances. In this study, to support work by regulatory and industrial researchers, simplified PBPK models for the organophosphorus pesticides acephate and chlorpyrifos and their primary metabolites were developed using a combination of algorithms, *in vivo* experimentation with chimeric mice with humanized livers, and literature resources. According to the current PBPK analysis, acephate cleared similarly from plasma in humans and mice, but accidental/incidental overdose levels of chlorpyrifos cleared more slowly from plasma in humans than it did in mice because its clearance is dependent on liver metabolism. The current data presented here illustrate how chimeric mice transplanted with human hepatocytes in combination with a simple PBPK model can assist evaluations of toxicological potential with respect to organophosphorus pesticides acephate and chlorpyrifos.

Conflict of interest disclosure statement

The authors declare that there are no conflicts of interest.

Acknowledgments

The authors thank Drs. Yasuhiko Ando, Shingo Kojima, Sayako Nishiyama, Ryohji Takano, and Norie Murayama for their technical assistance and David Smallbones for his English language advice. This work was supported in part by The Food Safety Commission of Japan (1103 to H.S. and H.Y.); the Ministry of Education, Culture, Sports, Science and Technology of Japan; and JCIA's LRI program.

References

Amidon, G.L., Sinko, P.J., Fleisher, D., 1988. Estimating human oral fraction dose absorbed: a correlation using rat intestinal membrane permeability for passive and carrier-mediated compounds. Pharm. Res. 5, 651–654.

Chang, A., Montesano, M.A., Barr, D., Thomas, J., Geller, R., 2009. Urinary elimination kinetics of acephate and its metabolite, methamidophos, in urine after acute ingestion. J. Med. Toxicol. 5, 68–72.

Drevenkar, V., Vasilic, Z., Stengl, B., Frobe, Z., Rumenjak, V., 1993. Chlorpyrifos metabolites in serum and urine of poisoned persons. Chem. Biol. Interact. 87, 315–322.

Edwards, S.W., Preston, R.J., 2008. Systems biology and mode of action based risk assessment. Toxicol. Sci. 106, 312–318.

Emoto, C., Murayama, N., Rostami-Hodjegan, A., Yamazaki, H., 2009. Utilization of estimated physicochemical properties as an integrated part of predicting hepatic clearance in the early drug-discovery stage: impact of plasma and microsomal binding. Xenobiotica 39, 227–235.

Foxenberg, R.J., Ellison, C.A., Knaak, J.B., Ma, C., Olson, J.R., 2011. Cytochrome P450-specific human PBPK/PD models for the organophosphorus pesticides: chlorpyrifos and parathion. Toxicology 285, 57–66.

Gargas, M.L., Andersen, M.E., Teo, S.K.O., Batra, R., Fennell, T.R., Kedderis, G.L., 1995. A physiologically based dosimetry description of acrylonitrile and cyanoethylene oxide in the rat. Toxicol. Appl. Pharmacol. 134, 185–194.

Hasegawa, M., Kawai, K., Mitsui, T., Taniguchi, K., Monnai, M., Wakui, M., Ito, M., Suematsu, M., Peltz, G., Nakamura, M., Suemizu, H., 2011. The reconstituted 'humanized liver' in TK-NOG mice is mature and functional. Biochem. Biophys. Res. Commun. 405, 405–410.

Higuchi, Y., Kawai, K., Yamazaki, H., Nakamura, M., Bree, F., Guillouzo, C., Suemizu, H., 2014. The human hepatic cell line HepaRG cells, possible cell source for steady generation of humanized liver TK-NOG mice. Xenobiotica 44, 146–153.

Hinderliter, P.M., Price, P.S., Bartels, M.J., Timchalk, C., Poet, T.S., 2011. Development of a source-to-outcome model for dietary exposures to insecticide residues: an example using chlorpyrifos. Regul. Toxicol. Pharmacol. 61, 82–92.

Joint FAO/WHO Meeting, 2003. Acephate. In: Pesticide Residues in Food – 2002. WHO, Geneva. pp. 3–36.

Kato, M., Shitara, Y., Sato, H., Yoshisue, K., Hirano, M., Ikeda, T., Sugiyama, Y., 2008. The quantitative prediction of CYP-mediated drug interaction by physiologically based pharmacokinetic modeling. Pharm. Res. 25, 1891–1901.

Lowe, E.R., Poet, T.S., Rick, D.L., Marty, M.S., Mattsson, J.L., Timchalk, C., Bartels, M.J., 2009. The effect of plasma lipids on the pharmacokinetics of chlorpyrifos and the impact on interpretation of blood biomonitoring data. Toxicol. Sci. 108, 258–272.

Mahajna, M., Quistad, G.B., Casida, J.E., 1997. Acephate insecticide toxicity: safety conferred by inhibition of the bioactivating carboxyamidase by the metabolite methamidophos. Chem. Res. Toxicol. 10, 64–69.

Marty, M.S., Andrus, A.K., Bell, M.P., Passage, J.K., Perala, A.W., Brzak, K.A., Bartels, M.J., Beck, M.J., Juberg, D.R., 2012. Cholinesterase inhibition and toxicokinetics in immature and adult rats after acute or repeated exposures to chlorpyrifos or chlorpyrifos-oxon. Regul. Toxicol. Pharmacol. 63, 209–224.

Montesano, M.A., Olsson, A.O., Kuklenyik, P., Needham, L.L., Bradman, A.S., Barr, D.B., 2007. Method for determination of acephate, methamidophos, omethoate, dimethoate, ethylenethiourea and propylenethiourea in human urine using high-performance liquid chromatography-atmospheric pressure chemical ionization tandem mass spectrometry. J. Expo. Sci. Environ. Epidemiol. 17, 321–330.

Raghu, P., Madhusudana, R.T., Reddaiah, K., Kumara Swamy, B.E., Sreedhar, M., 2014. Acetylcholinesterase based biosensor for monitoring of malathion and acephate in food samples: a voltammetric study. Food Chem. 142, 188–196.

Reiss, R., Neal, B., Lamb, J.C., Juberg, D.R., 2012. Acetylcholinesterase inhibition dose–response modeling for chlorpyrifos and chlorpyrifos-oxon. Regul. Toxicol. Pharmacol. 63, 124–131.

Renwick, A.G., 1993. Data-derived safety factors for the evaluation of food additives and environmental contaminants. Food Addit. Contam. 10, 275–305.

Smith, J.N., Hinderliter, P.M., Timchalk, C., Bartels, M.J., Poet, T.S., 2014. A human life-stage physiologically based pharmacokinetic and pharmacodynamic model for chlorpyrifos: development and validation. Regul. Toxicol. Pharmacol. 69, 580–597.

Smith, J.N., Timchalk, C., Bartels, M.J., Poet, T.S., 2011. In vitro age-dependent enzymatic metabolism of chlorpyrifos and chlorpyrifos-oxon in human hepatic microsomes and chlorpyrifos-oxon in plasma. Drug Metab. Dispos. 39, 1353–1362.

Takano, R., Murayama, N., Horiuchi, K., Kitajima, M., Kumamoto, M., Shono, F., Yamazaki, H., 2010. Blood concentrations of acrylonitrile in humans after oral administration extrapolated from *in vivo* rat pharmacokinetics, *in vitro* human metabolism, and physiologically based pharmacokinetic modeling. Regul. Toxicol. Pharmacol. 58, 252–258.

Tang, J., Cao, Y., Rose, R.L., Brimfield, A.A., Dai, D., Goldstein, J.A., Hodgson, E., 2001. Metabolism of chlorpyrifos by human cytochrome P450 isoforms and human, mouse, and rat liver microsomes. Drug Metab. Dispos. 29, 1201–1204.

Timchalk, C., Nolan, R.J., Mendrala, A.L., Dittenber, D.A., Brzak, K.A., Mattsson, J.L., 2002. A Physiologically based pharmacokinetic and pharmacodynamic (PBPK/PD) model for the organophosphate insecticide chlorpyrifos in rats and humans. Toxicol. Sci. 66, 34–53.

Timchalk, C., Poet, T.S., 2008. Development of a physiologically based pharmacokinetic and pharmacodynamic model to determine dosimetry and cholinesterase inhibition for a binary mixture of chlorpyrifos and diazinon in the rat. Neurotoxicology 29, 428–443.

Tsukada, A., Suemizu, H., Murayama, N., Takano, R., Shimizu, M., Nakamura, M., Yamazaki, H., 2013. Plasma concentrations of melengestrol acetate in humans extrapolated from the pharmacokinetics established in in vivo experiments with rats and chimeric mice with humanized liver and physiologically based pharmacokinetic modeling. Regul. Toxicol. Pharmacol. 65, 316–324.

Yamashita, M., Suemizu, H., Murayama, N., Nishiyama, S., Shimizu, M., Yamazaki, H., 2014. Human plasma concentrations of herbicidal carbamate molinate extrapolated from the pharmacokinetics established in *in vivo* experiments with chimeric mice with humanized liver and physiologically based pharmacokinetic modeling. Regul. Toxicol. Pharmacol. 70, 214–221.

Yamazaki, H., Horiuchi, K., Takano, R., Nagano, T., Shimizu, M., Kitajima, M., Murayama, N., Shono, F., 2010. Human blood concentrations of cotinine, a biomonitoring marker for tobacco smoke, extrapolated from nicotine metabolism in rats and humans and physiologically based pharmacokinetic modeling. Int. J. Environ. Res. Public Health 7, 3406–3421.

Yamazaki, H., Suemizu, H., Murayama, N., Utoh, M., Shibata, N., Nakamura, M., Guengerich, F.P., 2013. *In vivo* drug interactions of the teratogen thalidomide with midazolam: heterotropic cooperativity of human cytochrome P450 in humanized TK-NOG mice. Chem. Res. Toxicol. 26, 486–489.

Yamazaki, H., Suemizu, H., Shimizu, M., Igaya, S., Shibata, N., Nakamura, N., Chowdhury, G., Guengerich, F.P., 2012. *In vivo* formation of dihydroxylated and glutathione conjugate metabolites derived from thalidomide and 5-hydroxythalidomide in humanized TK-NOG mice. Chem. Res. Toxicol. 25, 274–276.

LIVER TRANSPLANTATION 20:1127–1137, 2014

ORIGINAL ARTICLE

Hepatocytes Buried in the Cirrhotic Livers of Patients With Biliary Atresia Proliferate and Function in the Livers of Urokinase-Type Plasminogen Activator–NOG Mice

Hiroshi Suemizu,[1]* Kazuaki Nakamura,[3]* Kenji Kawai,[2] Yuichiro Higuchi,[1] Mureo Kasahara,[4] Junichiro Fujimoto,[5] Akito Tanoue,[3] and Masato Nakamura[6]

[1]Biomedical Research Department, and [2]Pathology Research Department, Central Institute for Experimental Animals, Kanagawa, Japan; [3]Department of Pharmacology, [4]Department of Transplant Surgery, and [5]Clinical Research Center, National Center for Child Health and Development, Tokyo, Japan; and [6]Department of Pathology and Regenerative Medicine, Tokai University School of Medicine, Kanagawa, Japan

The pathogenesis of biliary atresia (BA), which leads to end-stage cirrhosis in most patients, has been thought to inflame and obstruct the intrahepatic and extrahepatic bile ducts. BA is not believed to be caused by abnormalities in parenchymal hepatocytes. However, there has been no report of a detailed analysis of hepatocytes buried in the cirrhotic livers of patients with BA. Therefore, we evaluated the proliferative potential of these hepatocytes in immunodeficient, liver-injured mice [the urokinase-type plasminogen activator (uPA) transgenic NOD/Shi-scid IL2rγnull (NOG); uPA-NOG strain]. We succeeded in isolating viable hepatocytes from the livers of patients with BA who had various degrees of fibrosis. The isolated hepatocytes were intrasplenically transplanted into the livers of uPA-NOG mice. The hepatocytes of only 3 of the 9 BA patients secreted detectable amounts of human albumin in sera when they were transplanted into mice. However, human leukocyte antigen–positive hepatocyte colonies were detected in 7 of the 9 mice with hepatocyte transplants from patients with BA. We demonstrated that hepatocytes buried in the cirrhotic livers of patients with BA retained their proliferative potential. A liver that was reconstituted with hepatocytes from patients with BA was shown to be a functioning human liver

Additional Supporting Information may be found in the online version of this article.

Abbreviations: 5-CF, 5-carboxyfluorescein; 5-CFDA, 5(6)-carboxyfluorescein diacetate; αSMA, alpha smooth muscle actin; ABC, adenosine triphosphate–binding cassette; ALB, albumin; BA, biliary atresia; BC, bile canaliculus; CFDA, 5-carboxyfluorescein diacetate; CYP, cytochrome P450; GAPDH, glyceraldehyde-3-phosphate dehydrogenase; hALB, human albumin; H&E, hematoxylin and eosin; HIF, high intrinsic fluorescence; HLA, human leukocyte antigen; IF, intrinsic fluorescence; LT, liver transplantation; MRP2, multidrug resistance–associated protein 2; ND, not detected by an enzyme-linked immunosorbent assay; NGS, normal goat serum; NMS, normal mouse serum; NR1, nuclear receptor subfamily 1; NRS, normal rabbit serum; PELD, Pediatric End-Stage Liver Disease; PI, propidium iodide; SLC, solute carrier family; UGT, uridine diphosphate glucuronosyltransferase; uPA, urokinase-type plasminogen activator; VIM, vimentin.

The authors report no conflicts of interest.

Hiroshi Suemizu was the primary experimenter, performed all transplants, analyzed the liver-reconstituted mice, and wrote the article. Kazuaki Nakamura, Mureo Kasahara, Junichiro Fujimoto, and Akito Tanoue performed all isolations of human hepatocytes and managed all the clinical samples. Kenji Kawai provided all the tissue histology. Yuichiro Higuchi analyzed the liver-reconstituted mice. Masato Nakamura provided overall project planning and coordination.

This work was supported in part by Grants-in-Aid for Scientific Research to Hiroshi Suemizu (21240042) and Akito Tanoue (23300162) from the Japan Science and Technology Agency.

*These authors contributed equally to this work.

Address reprint requests to Hiroshi Suemizu, Ph.D., Biomedical Research Department, Central Institute for Experimental Animals, 3-25-12 Tonomachi, Kawasaki-Ku, Kawasaki, Kanagawa 210-0821, Japan. Telephone: +81-44-201-8530; FAX: +81-44-201-8541 or +81-44-201-8511; E-mail: suemizu@ciea.or.jp or nogmouse@ciea.or.jp

DOI 10.1002/lt.23916
View this article online at wileyonlinelibrary.com.
LIVER TRANSPLANTATION.DOI 10.1002/lt. *Published on behalf of the American Association for the Study of Liver Diseases*

with a drug-metabolizing enzyme gene expression pattern that was representative of mature human liver and biliary function, as ascertained by fluorescent dye excretion into the bile canaliculi. These results imply that removing the primary etiology via an earlier portoenterostomy may increase the quantity of functionally intact hepatocytes remaining in a cirrhotic liver and may contribute to improved outcomes. *Liver Transpl 20:1127-1137, 2014.* © 2014 AASLD.

Received January 2, 2014; accepted May 10, 2014.

Biliary atresia (BA), the most common pediatric cholestatic disease, is caused by the progressive fibro-obliterative obstruction of the extrahepatic and intrahepatic bile ducts within the first few weeks of life.[1,2] The current surgical treatment is sequential. In the first few weeks of life, a Kasai portoenterostomy is performed to bypass the obstructed extrahepatic bile ducts and restore the biliary flow.[3] Approximately 20% of all patients who undergo portoenterostomy during infancy survive into adulthood with their native liver.[2,4] In general, it is advantageous to perform portoenterostomy as early after birth as possible to optimize the chance of success.[5] Patients who fail to undergo portoenterostomy experience a gradual deterioration of liver function and develop progressive fibrosclerosis; after the initial successful establishment of bile flow, liver transplantation (LT) is the only treatment option. Although several etiologies of BA have been postulated, the precise pathogenesis of BA remains unknown. Some factors that might contribute to its development are genetic, infective, inflammatory, and toxic insults.[1] In most cases, BA is associated with an intensive inflammatory infiltrate; this knowledge led us to the conjecture that BA results from an infectious or autoimmune destruction of the bile ducts. For example, the infection of newborn mice with the Rhesus rotavirus results in a BA-like disease.[6-8] Meanwhile, hepatocytes from patients with BA have not been thought to be involved in the development of chronic obstructive cholestasis. We and other groups have developed mice with humanized livers in which the liver is reconstituted with human hepatocytes so that in vivo drug metabolism and liver regeneration can be studied.[9-11] Therefore, the aims of this study were to evaluate the in vivo proliferative potential and functional properties of hepatocytes buried in the cirrhotic livers of BA patients.

MATERIALS AND METHODS

Specimens from the National Research Institute for Child Health and Development were collected in a standardized manner with the permission of the patients' families.

Animals

All mouse studies were conducted in strict accordance with *Guide for the Care and Use of Laboratory Animals* from the Central Institute for Experimental Animals. All experimental protocols were approved by the animal care committee of the Central Institute for Experimental Animals (permit number 11029A). All surgeries were performed under isoflurane anesthesia, and all efforts were made to minimize animal suffering. All studies using mouse tissue with transplanted human cells were approved by the ethics and biosafety committee of the National Research Institute for Child Health and Development and the Central Institute for Experimental Animals. The urokinase-type plasminogen activator (uPA) transgenic NOD/Shi-scid IL2rγnull (NOG); uPA-NOG strain[11] was maintained through the breeding of a female uPA-NOG hemizygote with a male homozygote. The zygosity of the *uPA* transgene was presumed from the degree of liver damage, which was examined through the determination of the serum levels of alanine aminotransferase with a Fuji DRI-CHEM 7000 clinical biochemical analyzer (Fujifilm Corp., Tokyo, Japan). The uPA-NOG mice with serum alanine aminotransferase activity greater than 150 U/L were selected as homozygotes and were then used as transplant recipients.

Isolation of Hepatocytes From the Livers of Patients With BA

The entire experimental protocol was approved by the ethics and research committee of the National Center for Child Health and Development. Written informed consent was obtained in each case. Except for the pieces of liver tissue that were used as pathological specimens, the enucleated diseased livers from the transplant recipients were discarded. The human hepatocytes used in this study were procured from liver tissue removed from BA patients who met the diagnostic criteria [Pediatric End-Stage Liver Disease (PELD) score[12] $\geq$ 6 points] for LT operations. The levels of fibrosis were categorized according to the following criteria: (I) mild (portal fibrous expansion to bridging fibrosis involving $\leq$50% of portal tracts), (II) moderate (bridging fibrosis involving >50% of portal tracts), and (III) severe (bridging fibrosis involving >50% of the portal tracts with nodular architectural changes).[13] Patient 141, who had grade III fibrosis and a PELD score of 0, had portopulmonary syndrome (intrapulmonary shunting). The shunt ratio, calculated with technetium-99m macroaggregated albumin (ALB) scintigraphy, was 16.8%, which indicated a relatively mild shunt. The hepatocytes were isolated from the resected liver tissue through the 2-step collagenase perfusion[14] of the liver samples, as described previously.[15] Hepatic parenchymal cells were isolated with low-speed centrifugation (50*g*). Cell numbers and viability were assessed with trypan blue exclusion.[16]

Flow Cytometry Analysis

The hepatocytes were stained with 1 mg/mL propidium iodide (PI; Sigma-Aldrich Co. LLC, St. Louis, MO), which stains dead cells. The intensity of 502-nm fluorescence was measured as intrinsic fluorescence (IF). Flow cytometry data were collected with a FACSCanto analyzer and BD FACSDiva software (BD Biosciences, Franklin Lakes, NJ). The data were analyzed with the FlowJo program (Tree Star, Inc., Ashland, OR).

Transplantation of Hepatocytes Into uPA-NOG Mice

Hepatocytes from patients with BA and commercially available cryopreserved human hepatocytes from a 4-year-old female (NHEPS, Lonza, Walkersville, MD) were used as donor cells. Young (8-week-old) male uPA-NOG mice were used as the recipients of the human hepatocytes. One million viable hepatocytes were injected intrasplenically via a Hamilton syringe with a 26-G needle. The successful engraftment of the human hepatocytes was evaluated through the measurement of the blood level of human albumin (hALB) with an hALB enzyme-linked immunosorbent assay quantitation kit (Bethyl Laboratories, Montgomery, TX) according to the manufacturer's protocol. The replacement index, which was the percentage of human donor hepatocytes in the recipient liver, was estimated according to the hALB concentration in chimeric mice.[17]

Histology and Immunohistochemistry

The tissues were fixed with 4% (vol/vol) phosphate-buffered formalin (Mildform, Wako Pure Chemical Industries, Ltd., Osaka, Japan), and 5-μm paraffin-embedded sections were stained with Azan-Mallory staining reagents (Muto Pure Chemicals, Tokyo, Japan) to visualize the collagen and muscle fibers and with hematoxylin and eosin (H&E). Some sections were autoclaved for 10 minutes in a target retrieval solution [0.1 M citrate buffer (pH 6.0) and 1 mM ethylene diamine tetraacetic acid (pH 9.0)] and were then equilibrated at room temperature for 20 minutes. Monoclonal mouse anti–human leukocyte antigen (anti-HLA) class I (A-C) antibodies (clone EMR8-5, Hokudo, Sapporo, Japan; 1:2000),[18] polyclonal goat anti-human ALB antibodies (Bethyl Laboratories; 1:1500), polyclonal rabbit anti-cytochrome P450 3A4 (CYP3A4) antibodies (Abcam, Inc., Cambridge, MA; 1:500), monoclonal mouse anti-human Ki-67 antigen antibodies (clone MIB-1; Dako Denmark A/S; 1:50),[19] monoclonal mouse anti-human multidrug resistance–associated protein 2 (MRP2) antibodies (clone M2 III-6, Millipore, Billerica, MA; 1:100),[20] monoclonal rabbit anti-vimentin (anti-VIM) antibodies (clone SP20, Nichirei Bioscience, Tokyo, Japan; 1:1500),[21] and monoclonal rabbit anti–alpha smooth muscle actin (anti-αSMA) antibodies (clone 1A4, Leica Microsystems, Tokyo, Japan; 1:200)[22] were used as primary antibodies. Normal mouse serum (NMS), normal goat serum (NGS), and normal rabbit serum (NRS) were used as negative controls for immunostaining. For bright-field immunohistochemistry, the antibodies for mouse, goat, and rabbit immunoglobulin were visualized with amino acid polymer/peroxidase complex–labeled antibodies [Histofine Simple Stain MAX PO (M, G, and R), Nichirei Bioscience) and a Bond Polymer Refine Detection system (Leica Microsystems) with a diaminobenzidine substrate [Dojindo Laboratories, Kumamoto, Japan; 0.2 mg/mL 3,3′-diaminobenzidine tetrahydrochloride, 0.05 M tris(hydroxymethyl)-aminomethane with hydrochloric acid (pH 7.6), and 0.005% hydrogen peroxide]. The sections were counterstained with hematoxylin. Hepatic biliary obstructions were examined with Hall's bilirubin staining method.[23] The images were captured under an Axio Imager upright microscope (Carl Zeiss, Thornwood, NY) equipped with AxioCam HRm and AxioCam MRc5 charge-coupled device cameras (Carl Zeiss).

Real-Time Quantitative Reverse-Transcription Polymerase Chain Reaction for Drug Metabolism–Related Gene Expression

The total cellular RNA was isolated from the livers with an RNeasy mini kit (Qiagen K.K.). Complementary DNA was synthesized with a high-capacity complementary DNA reverse transcription kit (Applied Biosystems, Foster City, CA) with random hexamers. TaqMan gene expression master mix and TaqMan gene expression assays (Applied Biosystems) were used for the real-time quantitative polymerase chain reactions; amplifications were performed with an ABI-Prism 7000 sequence detection system (Applied Biosystems). The comparative threshold cycle (Ct) method was used to determine the relative ratio of the gene expression for each gene, which was corrected with human glyceraldehyde-3-phosphate dehydrogenase (GAPDH) and referenced to the RNA extracted from donor hepatocytes. The TaqMan assay numbers are listed in Table 1.

Biliary Excretion Test With 5(6)-Carboxyfluorescein Diacetate (5-CFDA)

The ester precursor of 5-carboxyfluorescein (5-CF), 5(6)-carboxyfluorescein diacetate (5-CFDA; 0.5 nmol; Sigma-Aldrich), was injected intravenously into the mouse tail vein. Ten minutes after the 5-CFDA injection, the liver was perfused with 50 nmol/L 5-CFDA for 3 minutes, and the liver was then embedded in an optimum cutting temperature (O.C.T.) compound (Sakura Finetek Japan Co., Ltd., Tokyo, Japan) and frozen in liquid nitrogen. Ten-micrometer-thick serial frozen sections were prepared and air-dried. The 5-CF fluorescent signals were captured with an Axio Imager upright microscope (Carl Zeiss) equipped with AxioCam HRm and AxioCam MRc5 charge-coupled device cameras (Carl Zeiss). After the microfluorographs were taken, the tissue sections were fixed and rehydrated sequentially in decreasing concentrations of ethanol and water, and this was followed by immunohistochemical staining for MRP2. Sections were counterstained with

TABLE 1. TaqMan Probe Information

Gene Name	Gene Description	TaqMan Assay Number
GAPDH	Glyceraldehyde-3-phosphate dehydrogenase	Hs99999905_m1
ALB	Albumin	Hs99999922_s1
CYP1A1	Cytochrome P450, family 1, subfamily A, polypeptide 1	Hs00153120_m1
CYP1A2	Cytochrome P450, family 1, subfamily A, polypeptide 2	Hs00167927_m1
CYP2A6	Cytochrome P450, family 2, subfamily A, polypeptide 6	Hs00868409_s1
CYP2B6	Cytochrome P450, family 2, subfamily B, polypeptide 6	Hs03044634_m1
CYP2C8	Cytochrome P450, family 2, subfamily C, polypeptide 8	Hs00258314_m1
CYP2C9	Cytochrome P450, family 2, subfamily C, polypeptide 9	Hs00426397_m1
CYP2C18	Cytochrome P450, family 2, subfamily C, polypeptide 18	Hs00426400_m1
CYP2C19	Cytochrome P450, family 2, subfamily C, polypeptide 19	Hs00426380_m1
CYP2D6	Cytochrome P450, family 2, subfamily D, polypeptide 6	Hs00164385_m1
CYP2E1	Cytochrome P450, family 2, subfamily E, polypeptide 1	Hs00559368_m1
CYP3A4	Cytochrome P450, family 3, subfamily A, polypeptide 4	Hs00430021_m1
CYP3A5	Cytochrome P450, family 3, subfamily A, polypeptide 5	Hs00241417_m1
UGT1A1	Uridine diphosphate glucuronosyltransferase 1 family, polypeptide A1	Hs02511055_s1
UGT2B15	Uridine diphosphate glucuronosyltransferase 2 family, polypeptide B15	Hs00870076_s1
ABCB1	Adenosine triphosphate–binding cassette, subfamily B (MDR/TAP), member 1	Hs00184500_m1
ABCB11	Adenosine triphosphate–binding cassette, subfamily B (MDR/TAP), member 11	Hs00184824_m1
ABCC2	Adenosine triphosphate–binding cassette, subfamily C (CFTR/MRP), member 2	Hs00166123_m1
ABCG2	Adenosine triphosphate–binding cassette, subfamily G (WHITE), member 2	Hs01053790_m1
SLC22A1	Solute carrier family 22 (organic cation transporter), member 1	Hs00427552_m1
SLC22A7	Solute carrier family 22 (organic anion transporter), member 7	Hs00198527_m1
SLC22A9	Solute carrier family 22 (organic anion transporter), member 9	Hs00971064_m1
NR1H4	Nuclear receptor subfamily 1, group H, member 4	Hs00231968_m1
NR1I2	Nuclear receptor subfamily 1, group I, member 2	Hs00243666_m1
NR1I3	Nuclear receptor subfamily 1, group I, member 3	Hs00901571_m1

hematoxylin. Another tissue section was fixed in 4% paraformaldehyde, and this was followed by immunofluorescent staining with monoclonal mouse anti-HLA class I (A-C) antibodies, a streptavidin/Texas Red–labeled secondary antibody (GE Healthcare Bio-Sciences), and H&E. Commercially available cryopreserved human hepatocytes (normal hepatocytes) and cells from the HCT 116 line (American Type Culture Collection, Manassas, VA), a human colorectal carcinoma cell line that easily engrafts and forms tumor cell colonies in NOG mouse livers,[24] were used as positive and negative controls for the formulation of the bile canaliculus (BC) network.

Statistical Analyses

Group comparisons were performed with the Student *t* test for independent samples. *P* values less than 0.05 were considered significant (Prism 5, GraphPad Software, Inc., La Jolla, CA).

RESULTS

Engraftment of Hepatocytes From Patients With BA in uPA-NOG Mouse Livers

Using liver failure immunodeficient mouse models, we first evaluated the regenerative potential of the residual hepatocytes buried in the cirrhotic livers of patients with BA.[11] We succeeded in isolating viable hepatocytes from the livers of 9 BA patients with various degrees of fibrosclerosis (Table 2 and Fig. 1A). The typical gross morphology of a liver from a patient with BA is shown in Fig. 1B. There was no significant difference ($P = 0.45$) between the cell yields from patients with grade II fibrosis (2.3 ± 1.6 million cells per gram of liver, $n = 3$) and patients with grade III fibrosis (3.8 ± 4.2 million cells per gram of liver, $n = 6$; Fig. 1C). The cell viability was not significantly different ($P = 0.81$) between patients with grade II fibrosis ($76.7\% \pm 16.0\%$, $n = 3$) and patients with grade III fibrosis ($73.3\% \pm 23.0\%$, $n = 6$; Fig. 1D). The isolated hepatocytes were analyzed with flow cytometry (Fig. 1D). Because the IF signal of the hepatocytes from patients with BA was not increased in comparison with normal hepatocytes, it did not seem that bile accumulated within the hepatocytes, even in the patients with BA. The viable and engraftable hepatic parenchymal cells seemed to be present in the high intrinsic fluorescence (HIF) fraction; these cells had a very large cell mass and a complicated internal structure because the percentage of the HIF fraction correlated positively with the engraftability of the hepatocytes, which was based on the plasma concentration of hALB ($r^2 = 0.8784$; Fig. 1E, right). However, the cell viability did not show a direct correlation with the plasma concentration of hALB ($r^2 = 0.0515$; Fig. 1E, center) or the percentage of the HIF fraction ($r^2 = 0.0064$; Fig. 1E, left). The isolated hepatocytes were intrasplenically transplanted into uPA-NOG mice. Successful engraftment was evaluated in terms of the detection of hALB in the mouse serum

TABLE 2. Engraftment of Hepatocytes Derived From Patients With BA in uPA-NOG Mouse Livers

	Patient Information				Isolated Hepatocytes			Experimental Condition and Summarized Results			
										Animals With Engraftment	
Number	Age	Sex	Fibrosis Level	PELD Score	Cells/g of Liver	Viability (%)	HIF (%)	Condition*	Cell Dose (Cells/Mouse)	HLA-Positive Colony: [n/N (%)]†	hALB [n/N (μg/mL)]
80	10 months	Female	II	20	1.2×10^6	66	9.0	A	1.0×10^6	5/5 (100)	5/5 (230-875)
								B	1.0×10^6	4/4 (100)	1/4 (280)
								C	1.0×10^6	4/4 (100)	1/4 (38)
86	7 months	Female	II	35	1.5×10^6	95	4.8	A	1.0×10^6	2/2 (100)	1/2 (35)
								B	1.0×10^6	2/4 (50)	1/4 (105)
153	8 months	Male	II	9	4.1×10^6	69	1.3	B	1.0×10^6	2/3 (67)	0/3 (ND)
105	5 months	Female	III	13	1.2×10^7	83	8.5	B	1.0×10^6	4/4 (100)	4/4 (49-294)
133	6 months	Female	III	15	6.9×10^4	33	9.2	B	2.0×10^5	0/1 (0)	0/1 (ND)
141	12 years	Female	III	0	3.0×10^6	93	4.8	B	1.0×10^6	1/1 (100)	0/1 (ND)
149	8 months	Female	III	14	3.4×10^6	67	0.8	B	1.2×10^6	3/3 (100)	0/3 (ND)
151	5 months	Female	III	10	1.4×10^6	69	5.0	B	1.0×10^6	3/4 (75)	0/4 (ND)
154	6 months	Female	III	14	3.1×10^6	95	4.2	B	1.0×10^6	0/1 (0)	0/1 (ND)
77	32 years	Male	Normal	—	2.0×10^6	88	25.5	C	1.0×10^6	5/5 (100)	5/5 (35-1516)

*The conditions were as follows: (A) fresh hepatocytes (within the first 6 hours after isolation), (B) chilled hepatocytes (stored at 4°C for more than 16 hours and up to 24 hours), and (C) cryopreserved hepatocytes.
†Hepatocyte colonies that contained more than 20 HLA-positive cells in the cross-sections.

and the appearance of HLA-positive hepatocyte colonies in the liver tissue (Fig. 1F). Although detectable amounts of secreted hALB were found only in the sera of mice that had received hepatocyte transplants from 3 of the 9 BA patients, HLA-positive hepatocyte colonies were detected as a result of 7 of the 9 hepatocyte transplants from patients with BA.

The expression of drug-metabolizing enzymes, a marker of a fully matured liver, was analyzed with real-time quantitative polymerase chain reaction. Livers reconstituted with hepatocytes from 2 different patients with BA (patients 80 and 105) and commercially available cryopreserved hepatocytes (NHEPS) were then examined. The relative gene expression profiles of hepatocytes from patients with BA were similar to those of NHEPS hepatocytes (Fig. 1G). The expression levels of most of the genes were higher in the reconstituted livers versus the donor hepatocytes (Fig. 1H).

Next, we examined the expression of ALB, a major functional marker of biosynthesis in the liver, via immunohistochemical staining with human-specific antibodies in hepatocytes originating from patients with BA (Fig. 2A, top and middle). This hepatic lineage marker protein was expressed within the human hepatocyte colonies in the reconstituted-liver mice at levels comparable to those of the liver reconstituted with cryopreserved normal hepatocytes (patient 77; Fig. 2A, bottom). The expression of CYP3A4, which is the main drug-metabolizing enzyme found in the liver, was also observed within the colonies consisting of both hepatocytes from patients with BA (Fig. 2A, top and middle) and normal hepatocytes (Fig. 2A, bottom), but it did not show the zonal distribution observed in the fully reconstituted uPA-NOG liver with NHEPS hepatocytes (Fig. 2B). Most human hepatocytes originating from the patients with BA were present as small foci that appeared to grow by clonal expansion within the uPA-NOG mouse livers. This growth was quite similar to that of normal hepatocytes from patient 77. In addition, immunohistochemical nuclear staining of serial sections of the mouse livers with an antibody (MIB-1) against the human Ki-67 antigen[25,26] revealed that the proliferative potential of the hepatocytes from the patients with BA was preserved, as evidenced by the nuclear staining of the hepatocytes located at the edges of human hepatocyte colonies (Fig. 2A, top and middle). NGS, NRS, and NMS (nonimmune), which corresponded to the host animals in which anti-ALB, anti-CYP3A4, and anti-Ki-67 antibodies, respectively, were prepared, did not react with either human or mouse hepatocytes (Fig. 2C). The hepatocyte colonies derived from the patients with BA were not stained by Azan-Mallory staining (Fig. 2A, top and middle).

Functional Integrity of Partially Humanized Livers

We confirmed the expression of MRP2 proteins on the plasma membranes of hepatocytes in both the livers of patients with BA and the partially humanized livers repopulated with hepatocytes from patients with BA

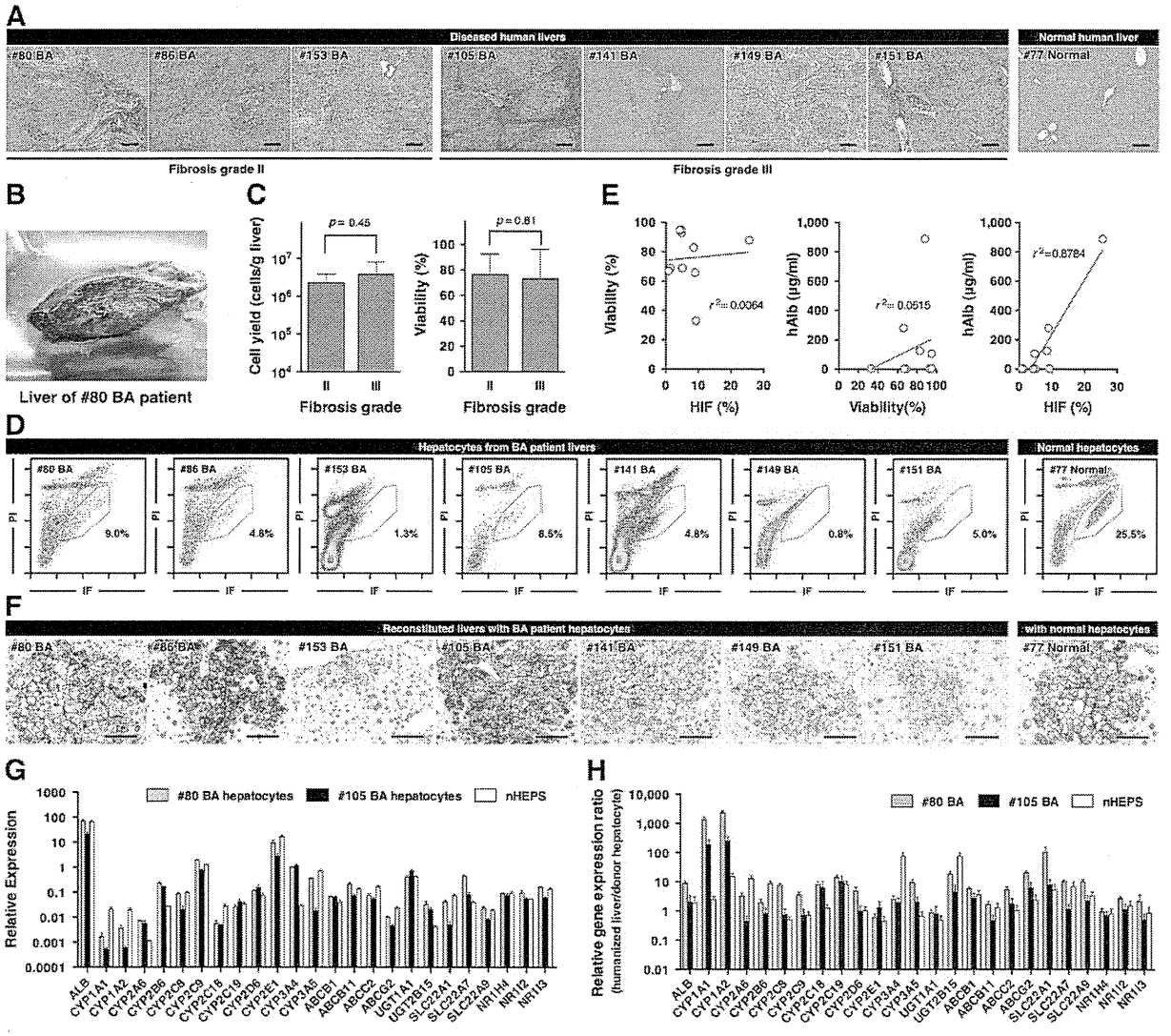

Figure 1. Engraftment of hepatocytes from BA patients in uPA-NOG mouse livers. (A) Azan-Mallory staining of 7 individual liver biopsy samples from BA patients and a healthy donor (normal). The scale bars represent 200 μm. (B) Gross morphology of the liver from BA patient 80. (C) Comparison of the cell yields and viability with grade II hepatic fibrosis and grade III hepatic fibrosis. (D) Isolated hepatocytes were analyzed with flow cytometry. Each HIF fraction is surrounded by a magenta border. (E) Correlation analyses of the cell viability, the HIF fraction percentage, and the hALB plasma concentration. (F) The engraftment of hepatocytes isolated from the BA patients and the healthy donors was confirmed with anti-human HLA staining. The scale bars represent 50 μm. (G) The relative expression levels of 24 human drug metabolism–related messenger RNAs in hepatocytes from BA patients and NHEPS hepatocytes were corrected with GAPDH. (H) The relative ratio of the gene expression for each reconstituted liver was referenced to the RNA extracted from the donor hepatocytes.

(Fig. 3A,B,). The cholestasis, visualized with Hall's bilirubin staining, was observed in many BCs in the livers of patients with BA (Fig. 3A, right). In contrast, the colonies repopulated with hepatocytes from patients with BA within the host mouse livers did not accumulate bile within their BCs (Fig. 3B). Azan-Mallory staining and VIM and αSMA antibody staining revealed fibrosis in the livers of patients with BA (Fig. 3C), but no fibrosis was observed within the colony repopulated with hepatocytes from patients with BA (Fig. 3D). We wondered whether these hepatocytes could reconstitute the functionally integrated BC network within the host mouse liver; therefore, we assessed the transporter function within the colonies of hepatocytes from patients with BA with 5-CFDA, a fluorescent marker used to visualize biliary excretion into BCs. After it is administered, 5-CFDA enters hepatocytes and is metabolized into 5-CF. This compound is excreted into BCs through the organic anion transporter MRP2.[27] Within the first 15 minutes after the administration of 5-CFDA, the hepatocytes from patients with BA in the uPA-NOG mice excreted 5-CF into the BCs, and it formed honeycomb networks surrounding individual hepatocytes (Fig. 4, top). This